7-25-2023

Early Chromosome Condensation By XIST Builds A-Repeat RNA Density That Facilitates Gene Silencing

M. Valledor

M. Byron

B. Dumas

See next page for additional authors

Recommended Citation

M. Valledor, M. Byron, B. Dumas, Dawn M. Carone, L. L. Hall, and J. B. Lawrence. (2023). "Early Chromosome Condensation By XIST Builds A-Repeat RNA Density That Facilitates Gene Silencing". *Cell Reports.* Volume 42, Issue 7. DOI: 10.1016/j.celrep.2023.112686
https://works.swarthmore.edu/fac-biology/653

Cell Reports

Article

Early chromosome condensation by XIST builds A-repeat RNA density that facilitates gene silencing

Graphical abstract

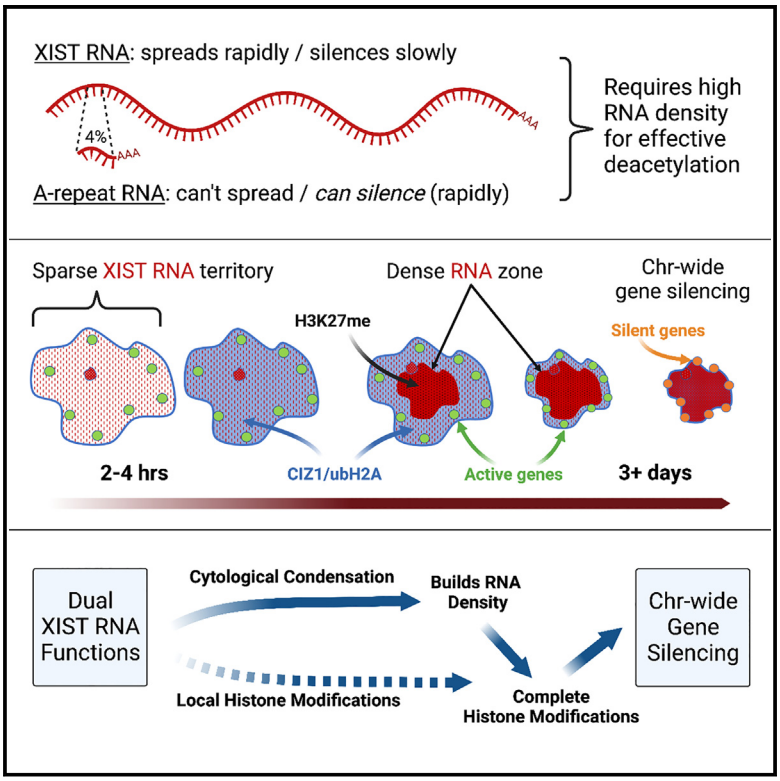

Highlights

- Sparse XIST transcripts spread widely and trigger UbH2A and CIZ1 in just 2–4 h
- XIST condenses architecture into a Barr body before chromosome-wide gene silencing
- A-repeat alone can silence genes where high local RNA density favors histone deacetylation
- Condensation builds RNA density supporting an unstable step required for stable silencing

Authors

Melvys Valledor, Meg Byron, Brett Dumas, Dawn M. Carone, Lisa L. Hall, Jeanne B. Lawrence

Correspondence

lisa.hall@umassmed.edu (L.L.H.), jeanne.lawrence@umassmed.edu (J.B.L.)

In brief

Valledor et al. show that XIST lncRNA condenses cytoarchitecture before widespread gene silencing. Surprisingly, tiny A-repeat RNA alone can rapidly silence local transcription, but only at high density. Results support that XIST impacts scaffold factors early to build a dense RNA/DNA territory, which promotes an A-repeat-dependent step required for silencing.

Valledor et al., 2023, Cell Reports *42*, 112686
July 25, 2023
https://doi.org/10.1016/j.celrep.2023.112686

CellPress

Cell Reports

CellPress
OPEN ACCESS

Article

Early chromosome condensation by XIST builds A-repeat RNA density that facilitates gene silencing

Melvys Valledor,[1,5] Meg Byron,[1] Brett Dumas,[2] Dawn M. Carone,[3] Lisa L. Hall,[1,*] and Jeanne B. Lawrence[1,4,6,*]
[1]Department of Neurology, University of Massachusetts Chan Medical School, Worcester, MA 01655, USA
[2]Department of Medicine, Boston University Medical Center, Boston, MA 02118, USA
[3]Department of Biology, Swarthmore College, Swarthmore, PA 19081, USA
[4]Department of Pediatrics, University of Massachusetts Chan Medical School, Worcester, MA 01655, USA
[5]Present address: Carbon Biosciences, Waltham, MA 02451, USA
[6]Lead contact
*Correspondence: lisa.hall@umassmed.edu (L.L.H.), jeanne.lawrence@umassmed.edu (J.B.L.)
https://doi.org/10.1016/j.celrep.2023.112686

SUMMARY

XIST RNA triggers chromosome-wide gene silencing and condenses an active chromosome into a Barr body. Here, we use inducible human XIST to examine early steps in the process, showing that XIST modifies cytoarchitecture before widespread gene silencing. In just 2–4 h, barely visible transcripts populate the large "sparse zone" surrounding the smaller "dense zone"; importantly, density zones exhibit different chromatin impacts. Sparse transcripts immediately trigger immunofluorescence for H2AK119ub and CIZ1, a matrix protein. H3K27me3 appears hours later in the dense zone, which enlarges with chromosome condensation. Genes examined are silenced after compaction of the RNA/DNA territory. Insights into this come from the findings that the A-repeat alone can silence genes and rapidly, but only where dense RNA supports sustained histone deacetylation. We propose that sparse XIST RNA quickly impacts architectural elements to condense the largely non-coding chromosome, coalescing RNA density that facilitates an unstable, A-repeat-dependent step required for gene silencing.

INTRODUCTION

Transcriptional silencing of one X chromosome in mammalian females is a pre-eminent model for epigenetic programming of facultative heterochromatin, a type of stable gene regulation inherited from cell to cell. The X-linked human *XIST* or mouse *Xist* gene produces a long (14–17 kb) non-coding RNA that coats the X chromosome in *cis*, triggering a cascade of repressive histone modifications for chromosome-wide gene silencing. This process not only silences active genes but transforms the active chromosome territory to the condensed, heterochromatic Barr body.[1–3] Many studies have shown that Xist RNA recruits numerous histone modifications, although it remains unclear which specific changes silence gene transcription. This study capitalizes on a robust model system to define changes immediately following *human* XIST RNA expression and thereby illuminate key questions not understood for either human or mouse XIST/Xist. A distinctive goal and contribution of this study is to examine early changes directly in the structural context in which XIST RNA functions: the architecture of a nuclear chromosome territory.

Cytological chromosome condensation might occur as a by-product of collective silencing of numerous active genes across a whole chromosome. However, long ago we raised "the Barr body paradox": why would such a large dense body be formed by local condensation of active genes which comprise only ~10% of chromosomal DNA in a given cell type?[4,5] More recently we showed that repeat-rich, non-coding CoT-1 heterogeneous nuclear RNA (hnRNA), which includes many low-level long non-coding RNAs (lncRNAs), contribute to an insoluble ribonucleoprotein (RNP) scaffold that promotes decondensed euchromatin. Hence, XIST RNA may induce chromosome condensation by impacting this repeat-rich RNP scaffold.[6] Furthermore, active coding genes are non-randomly organized in the geography of chromosome territories, which are composed largely of non-coding DNA.[7,8] Hence, to understand the whole process in the context in which it occurs, we visualize spatiotemporal relationships between human XIST RNA distribution, major histone modifications, silencing of specific genes, and changing chromosome architecture. This provides a window into poorly understood aspects of nuclear chromosome structure and epigenome regulation.

Most studies have investigated mouse Xist function, using female mouse embryonic stem cells (mESCs) or inducible transgenic systems. Transcriptional regulation of XIST/Xist is itself highly

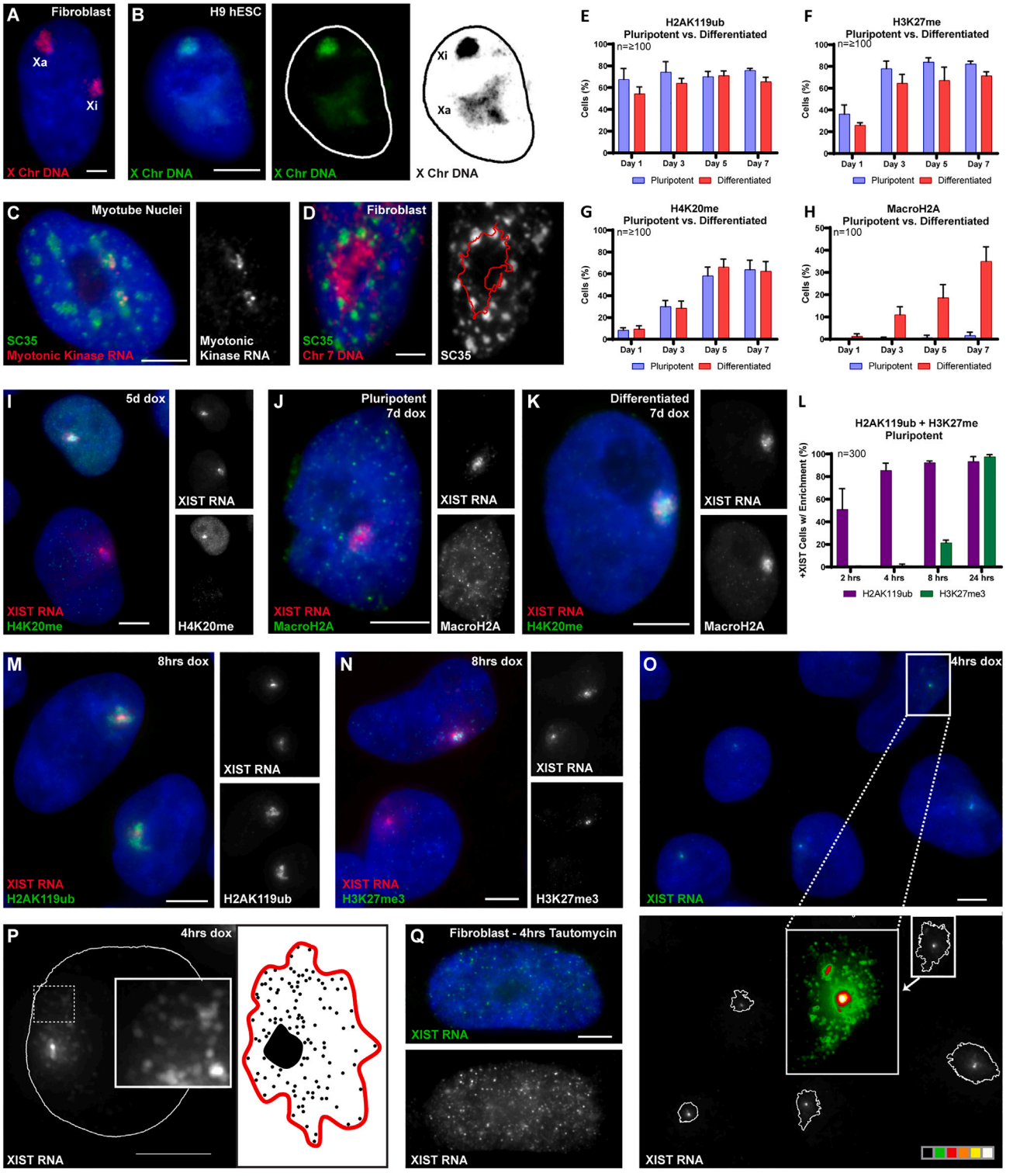

Figure 1. Human XIST RNA spreads rapidly and triggers sequential changes across an initially decondensed chromosome territory

(A and B) In somatic cells the size of Xa and Xi DNA territories are similar (A), whereas in pluripotent cells active chromosome territories are initially much more decondensed (B).

(C and D) Organization of genes in chromosome territories is non-random. Active genes/pre-mRNAs preferentially associate with SC-35 speckles (C), which are at the periphery of chromosome territories (D; outlined in red).

(legend continued on next page)

complex, with known species differences.[9,10] Notably, cultured human *in vitro* fertilized (IVF) embryos show initial biallelic XIST expression that switches to monoallelic expression prior to full chromosome silencing.[11,12] Because human female ESCs or induced pluripotent stem cells (iPSCs) show anomalies in XIST expression and X-inactivation,[13–18] some studies examine XIST in transformed cell lines, but XIST function is also compromised in this context. Here, study of human XIST RNA function is enabled by a human iPSC system carrying a single inducible XIST cDNA (14 kb) targeted into one trisomic chromosome 21 (chr21), which induces comprehensive chromosome-wide gene silencing and the Xi heterochromatin hallmarks on a chr21 "Barr body."[19–21] Importantly, silencing a trisomic chromosome circumvents creation of a functional monosomy or nullisomy that selects against cells with full XIST function; this likely contributes to incomplete silencing seen in some mouse Xist transgene studies.[22] In the trisomic iPSC system, XIST RNA fully silences the extra autosome,[21] in a several-day timeframe similar to that seen for natural X-inactivation in mESCs.[23] This provides a tractable system to study the process whereby human XIST RNA fully silences a human chromosome, beginning in developmentally appropriate pluripotent cells. As in mouse, in our system XIST expression is monoallelic from the beginning; however, our results suggest insights relevant to delayed chromosome silencing in IVF embryos, as will be discussed.

Despite much progress, it remains poorly understood which specific changes silence gene transcription,[24] and the potential functional role of changing chromosome architecture has received less attention. Beginning at just 2 h, we examine RNA distribution in direct relation to changes on individual chromosomes at three levels: biochemical, structural, and transcriptional. Among several findings, the first part of this study shows that very sparse XIST transcripts spread and act quickly, leading to large-scale condensation of the DNA/RNA territory, which, importantly, precedes silencing of the several active genes examined. A proposed concept that may explain this delay in gene silencing comes from the second part of the study revealing that a tiny XIST "minigene," containing just the "A-repeat" domain (~450 bp), can itself silence local gene transcription. Numerous mouse studies establish that deletion of the A-repeat prevents gene silencing[25–28]; however, it was not anticipated that this tiny fragment alone could silence endogenous genes without 96% of the long XIST transcript. Just one study examined the A-repeat alone in a somatic cell line and concluded that silencing of endogenous genes required other XIST domains[29]; however, here we re-examine this question in an iPSC developmental context that fully supports XIST RNA function. We show that the small A-repeat domain is itself sufficient to initiate local gene silencing of the several neighboring chromosomal genes examined. Other XIST domains are required for sparse RNA to spread across and condense the large territory into the Barr body. We further show that A-repeat silencing requires histone deacetylase activity, and this critical step for gene silencing is RNA density dependent and quickly reversible. The concept that initiation of gene silencing by XIST/A-repeat is RNA density dependent leads us to propose a model whereby earlier condensation of the chromosome coalesces a dense RNA territory that facilitates A-repeat function in chromosome-wide gene silencing. Results further suggest that XIST RNA function includes early and direct impact on non-histone architectural elements of the chromosome territory in addition to triggering histone modifications.

RESULTS

To investigate the inter-relationships between spread of human XIST RNA and changes to overall architecture, histone modifications, and transcriptional gene silencing, we examined RNA, DNA, and proteins on individual inactivating chromosomes in human iPSCs using molecular cytology. The importance of understanding XIST RNA function in the direct nuclear context is best appreciated by recognizing two major aspects of chromosome territory architecture. The first concerns the initial size of the territory across which XIST transcripts must spread and the magnitude of overall condensation induced by XIST. As typically observed in somatic cells, the inactive X chromosome (Xi) DNA territory appears only modestly smaller than the active X chromosome (Xa) (Figure 1A), but the process begins in pluripotent cells which have highly decondensed chromatin. As illustrated in human H9 ESCs,[17] the Xa territory is strikingly decondensed and large compared with the compacted Xi (Figure 1B). A second important structural consideration is that chromosomes comprise mostly non-coding DNA and the canonical genes are non-randomly organized; as we earlier showed, many active genes congregate with nuclear speckles rich in SC35 and splicing factors (Figure 1C),[5,30,31] as affirmed in genomic-scale studies.[8,32] Since speckles typically reside in interchromosomal regions (Figure 1D), the more active genes and pre-mRNA transcription is largely in the territory periphery.[33,34] These considerations provide important perspective for findings presented below: XIST RNA must function across broad physical space to enact large-scale structural transformation and silence active genes chromosome-wide.

Human XIST RNA triggers H2AK119ub within 2 h followed by H3K27me3, H4K20me, and macroH2A

To examine distinct steps in the process, we synchronously induced XIST on chr21, which comprehensively silences the

(E–K) (E–H) Histone marks triggered by human XIST RNA over a 7-day time course (comparing pluripotent and differentiating cells). In this experiment the marks were scored without an XIST reference and not all cells expressed XIST with dox induction. (I–K) Example images.
(L–N) (L) Hourly time course of H2AK119ub and H3K27me3 quantified with XIST RNA in expressing cells, with example images shown in (M) and (N).
(O) Very sparse XIST transcripts spread rapidly across large nuclear territory that can be masked by DAPI stain, thus sparse XIST paints are outlined below. Heatmap of enlarged territory in inset (for more details see supplemental information).
(P) Sparse XIST transcripts create punctate signals, as evident in inset and marked in schematic on the right.
(Q) Fully dispersed XIST transcripts released from chromosome by tautomycin.
DNA (DAPI) is in blue. Error bars denote SD from the mean. See STAR Methods for information on replicates. Scale bars, 5 μm.

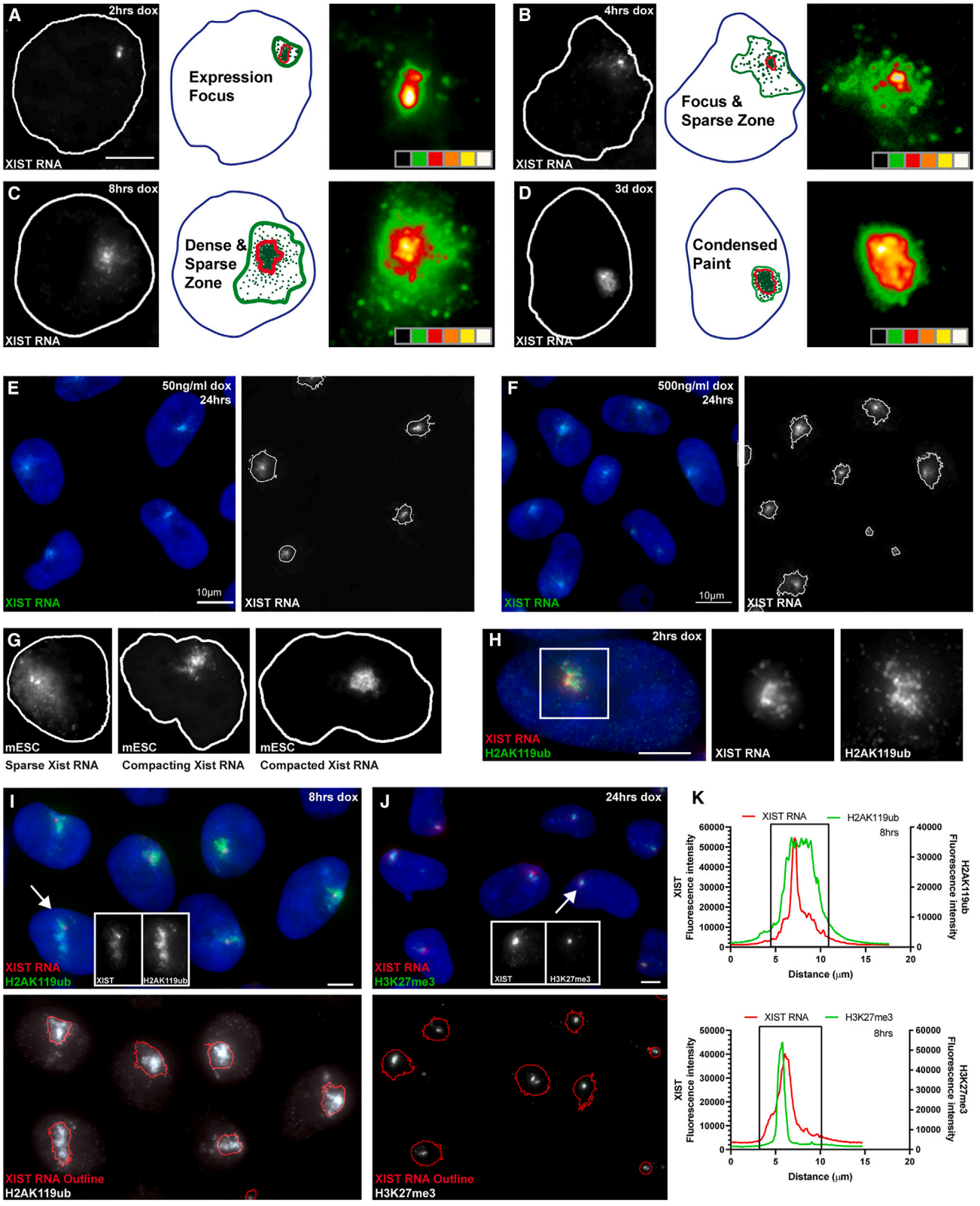

(legend on next page)

~300 genes across the chromosome in both pluripotent[19,21] and neural differentiated cells,[20] and compacts the chr21 territory (Figure S1A). For days 1–7 we visualized with XIST RNA four canonical heterochromatin hallmarks, H3K27me3, H2AK119ub, H4K20me and macroH2A, for which immunofluorescence allows sensitive detection of bright signals against a dark nuclear background, clearly indicating a territory enriched for that chromatin modification (e.g., Figures 1I–1K, 1M, and 1N).

We initially compared cells maintained as pluripotent or allowed to differentiate after XIST induction, which would reveal whether timing or presence of any of these modifications is differentiation dependent. Interestingly, all marks appeared with similar kinetics in pluripotent versus differentiating cells, except for macroH2A, which generally accumulated after the switch to differentiation conditions (Figures 1E–1H), although there was some variability in this (Figures S1B and S1C). Even in differentiating cultures, macroH2A lagged H4K20me by about 2 days, hence macroH2A is later and more differentiation dependent (Figures 1G–1K). H4K20me and macroH2A appear after H2AK119ub and H3K27me3, which are detected by day 1 independent of differentiation (Figures 1E–1H).

To assess whether H2AK119ub or H3K27me3 comes first, we examined cells just 2, 4, and 8 h post induction. Since not all cells induce XIST (due to transgene silencing), in this analysis we scored only XIST-expressing cells. Earlier reports in mouse suggested that Xist RNA recruits PRC2 first (for H3K27me3), followed by PRC1 (for H2AK119ub),[35] reflecting their canonical relationship, while subsequent studies report that H2AK119ub enriched first.[36,37] We see a clear temporal difference, with H2AK119ub enriched in 71%, 93%, and 98% of cells at just 2, 4, and 8 h, respectively (Figures 1L and 1M). In contrast, only ~24% of cells showed H3K27me3 enrichment by 8 h (Figures 1L and 1N), affirmed in multiple experiments (and different XIST transgenic clones). Hence, human XIST RNA triggered H2AK119ub several hours before H3K27me3, consistent with evidence that PRC1 is already present.[22,36,38]

XIST RNA rapidly spreads and triggers H2Aub across large "sparse zone," while H3K27me3 concentrates in small "dense zone"

Examination of XIST RNA 2 h after adding doxycycline (dox) revealed how rapidly XIST transcripts spread across a large but discrete nuclear territory. XIST quickly forms a small intense transcription focus, but sensitive RNA fluorescence *in situ* hybridization (FISH) also consistently detects very low levels of XIST transcripts that spread much further within 4 h, defining a much larger (~10–20×) than the bright RNA focus (Figures 1O, 1P, and 2A–2D). These sparse transcripts are visible through the microscope but are masked by DAPI staining or digital imaging often dominated by brighter signal (Figure 1O); sparse transcripts are seen at early time points and their detection requires optimal RNA preservation, hybridization, and detection. By 4 h most cells show this larger region of sparse punctate signal we term the "sparse zone," which surrounds a smaller bright RNA accumulation (including transcription focus), the "dense zone," with this consistent pattern evident in large fields of cells (Figure S1D). Sparse transcripts spread in a delimited region, unlike fully dispersed XIST RNA released from chromatin by brief (4 h) treatment with tautomycin[39] (Figure 1Q). Computer-generated heatmaps also demonstrate this larger low-intensity zone (~5× lower) (Figures 1O, S1D, and 2A–2C), although quantifying this is difficult because the sparse-zone signal is distinctly punctate (Figures 1O and 1P), unlike the more "solid" dense RNA territory at later times (Figures 2D and S1E). In Figures 1P and 2 a dot marks each punctum, with a distribution similar to a recent report estimating 50–200 XIST transcripts.[40] Our FISH results indicate XIST puncta in this upper range, and 200–300 transcripts per cell is consistent with our estimates (not shown) of XIST RNA relative to known abundant transcripts in our RNA-sequencing (RNA-seq) data.[21]

An important point is that XIST RNA levels plateau early; hence, cytological RNA density is built by compaction and not more transcription. Rodermund et al. reported that Xist RNA levels plateau after ~5 h and concluded that there are limited binding sites and unbound transcripts which rapidly degrade.[40] Supporting this, our microfluorimetry of RNA signals (see STAR Methods) showed no substantial change between 24 h and 7 days. The degradation of unbound transcripts likely explains why XIST RNA FISH appears so similar between individual cells, cell types, and even different model systems, including between human H9 ESCs and our inducible transgenic iPSCs (Figures S2A–S2C), our different transgenic clones (Figures S2E and S2F), and pluripotent versus differentiated cells. To assess whether XIST transcription level impacts RNA distribution, we varied dox concentrations over a 20-fold range (from 50 to 1,000 ng/mL); as shown in Figures 2E, 2F, and S2G, the same pattern of large sparse and small dense zones was seen (as with the 500 ng/mL routinely used). In addition, we quantified large RNA sparse zones that compacted with time in mESCs induced for transgenic Xist[41] (Figures 2G and S2H), and preliminary observations also suggest that this may occur in asynchronous mouse embryos (Figures S2I and S2J).

Most importantly, findings here make the critical point that these very sparse transcripts are not just inconsequential drifting RNA: they rapidly interact and modify chromatin. In just 2–4 h, H2AK119ub brightly decorates the whole XIST RNA territory including the sparse zone (Figures 2H, 2I, 2K, and S3A–S3C), a

Figure 2. Sparse XIST transcripts spread broadly within hours and alter chromatin differently in regions of high and low density

(A–D) XIST RNA rapidly spreads away from transcription focus at low levels across distended chromosome territory during the first hours of dox induction. The small XIST "dense zone" (A–C: red line in drawing) expands until a large condensed XIST RNA paint encompasses the chromosome (D). Heatmaps of XIST RNA FISH, on the right, demarcate low-intensity zones in green and high-density zones in red to white.

(E and F) Sparse XIST RNA zone is also detected at lower dox concentration.

(G) Sparse Xist RNA zone seen on transgenic mESC chromosome territories.

(H–K) Very low-level XIST RNA immediately triggers broad H2AK119ub modification, whereas H3K27me3 concentrates with dense zone. Broad H2AK119ub vs. limited H3K27me3 relative to XIST RNA distribution is further evident in line scans (K).

DNA (DAPI) is in blue. See STAR Methods for information on replicates. Scale bars, 5 μm.

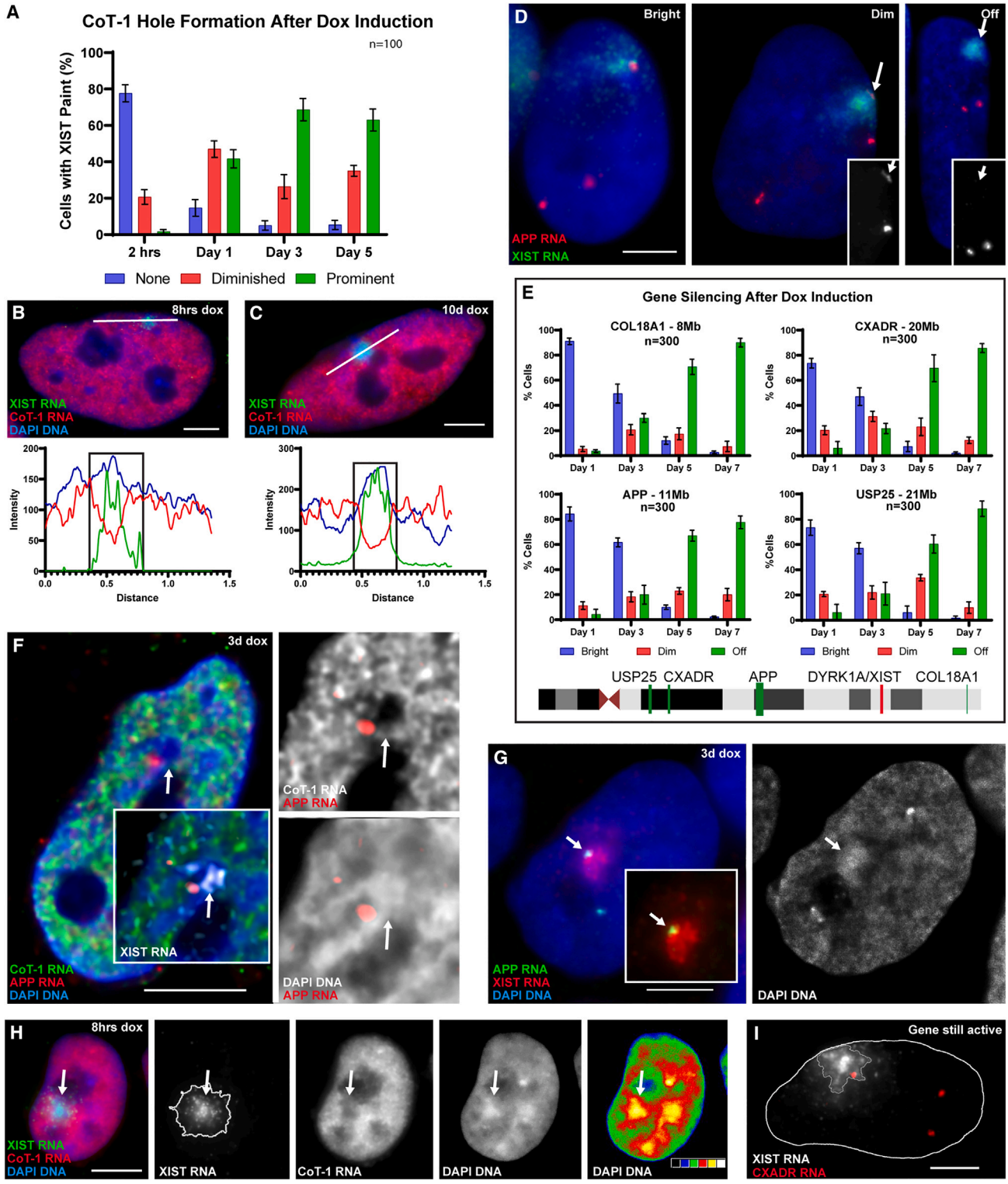

Figure 3. Formation of Barr body architecture occurs 1–2 days before complete gene silencing

(A, C, and F) Lack of bright CoT-1 RNA signal reliably delineates the condensed Barr body.

(A–C) Prominent "CoT-1 RNA holes" (absent CoT-1 RNA over XIST RNA signal) are formed in many cells by day 1 of XIST induction and reach maximal by day 3. At 8 h, CoT-1 RNA loss is primarily in the small dense RNA zone, coincident with more dense DNA, as indicated by V-shape in the linescan (in linescans in B and C, black boxes indicate XIST RNA territory).

(legend continued on next page)

consistent pattern shown in large fields of cells (Figure S3A). H2A ubiquitination shows striking spatial and temporal connection to barely detectable XIST RNA. In contrast, H3K27me3 appears later, more limited to the dense zone (Figures 2J, 2K, S3D, and S3E). As further evidenced below, these findings provided the initial indication that cytological density of RNA within the territory is a determinant of its impact on that region, with RNA density less limiting for H2AK119ub than H3K27me3.

We conclude that the sparse zone shown here comprises functional XIST transcripts that quickly spread and modify a larger nuclear territory than may be widely recognized. Results point to RNA density distribution in the chromosome territory as a significant parameter that influences its functional effects.

XIST RNA triggers condensation of the DNA/RNA territory before chromosome-wide gene silencing

In addition to silencing genes, XIST triggers compaction of the DNA/RNA territory to form the Barr body painted by a dense accumulation of XIST RNA. We examined the temporal relationship between gene silencing and changes to large-scale architecture in three ways: coalescence of the RNA territory, DNA condensation into the Barr body, and formation of the CoT-1 RNA void that marks the Barr body. Between days 1 and 3 the sparse zone coalesces into the uniformly dense XIST RNA accumulation typical of somatic cells by day 3 (Figures 2A–2D, S1D, and S1E), coinciding with Barr body formation.[42] Hence, cytological density of XIST RNA increases via chromosome contraction.

The Barr body is visible in many cells by DNA stain (DAPI), but percent detection varies between preparations (Figures S4A–S4C). Therefore, we used the CoT-1 RNA assay, which several studies show reliably delineates the Barr body (Figures S4D–S4G). CoT-1 RNA coats decondensed euchromatin but is depleted from heterochromatin, forming a distinct "CoT-1 RNA hole" over the Barr body[6,43–45] (e.g., Figures 3C and 3F). Scoring CoT-1 RNA at different time points (Figures 3A–3C), we found that by day 1 a CoT-1 RNA hole/Barr body was seen in many cells, and by day 3 this was as prominent (and frequent) as at day 5. While significant CoT-1 RNA loss over the inactivating chromosome was often apparent at day 1, at earlier hours only a small subset of cells showed any discernible CoT-1 RNA loss, primarily in the small dense zone (Figures 3B, S4D, and S4E), where DNA condensation apparently begins (Figures 3H and S4H).

On parallel slides we scored silencing of several protein-coding genes using RNA FISH to detect allele-specific expression of transcription foci (TFs)[30,44] (Figures 3D and 3E). Using genomic probes for four active genes which map widely across the chromosome (Figure 3E), we quantified silencing at days 1, 3, 5, and 7. In contrast to substantial CoT-1 RNA reduction at day 1, all four genes continued to exhibit TFs from the XIST-associated allele in these rapidly dividing cells. Appreciable silencing was not seen until day 3 when many cells still exhibited TFs (Figures 3F, 3G, and S4I–S4L), in contrast to full silencing after day 5 (Figure 3E). Hence, using CoT-1 RNA loss as a proxy for the Barr body, architectural condensation occurs prior to silencing genes examined.

These results predict that at day 3 many cells still have TFs associated with a prominent Barr body. This was directly shown in individual cells dual-labeled with DAPI-DNA showing a dense body coincident with a CoT-1 RNA void, which is also associated with a transcription focus for the APP gene (Figures 3F, S4I, and S4J). In samples with favorable DAPI staining (Figures 3G, S4K, and S4L), 83% of cells showed a DAPI-dense Barr body at day 3, and half (49%) of these Barr bodies were still associated with a transcription focus. This further demonstrates chromosome compaction before gene silencing, reinforcing the kinetics of CoT-1 RNA/gene silencing in the cell population (Figures 3B, 3G, and 3I). Thus, chromosome condensation begins early and is essentially complete about a day before long-range silencing of the canonical genes.

XIST rapidly impacts CIZ1 and may directly affect architectural scaffold proteins

The aforementioned findings show a substantial lag between rapid spread of XIST RNA and gene silencing, during which cytological-scale condensation occurs. While histone modifications are heavily studied, lncRNAs can also serve an architectural role in forming cytological-scale structures, as reviewed by Smith et al.[8] We earlier suggested that XIST RNA is bound with a nuclear matrix[42] and recently developed a more selective nuclear fractionation to demonstrate that XIST RNA is embedded with an insoluble RNP scaffold/matrix, which persists independent of DNA removal.[6] SAF-A and CIZ1 are two matrix proteins thought to tether XIST RNA to localize histone modifications[46–48]; however, XIST RNA function could include more direct effects on nuclear architectural elements.

SAF-A is known to be broadly present across chromatin of somatic cells, and we show a similar distribution in iPSCs (Figure 4A). CIZ1 is also widely expressed, but we found that iPSCs lack significant CIZ1 staining prior to XIST induction (Figure 4B). Upon induction, a bright CIZ1 territory rapidly appears within just 2 h across both sparse and dense zones where there is any trace of RNA (Figures 4B–4D). Costaining of CIZ1 and H2AK119ub showed both CIZ1 and H2AK119ub in the large sparse RNA territory, and scoring showed essentially indistinguishable rapid kinetics (Figures 4C, 4E, and S5A). In contrast, costaining with H3K27me3 showed that CIZ1 appears first, in a region ~2.5 times larger than H3K27me3 (Figures 4F, 4G, and S5B–S5E), and a slight punctate H3K27me3 signal was only occasionally evident in the sparse zone at early time points (Figure S5D).

Given the lack of CIZ1 staining before induction, it was surprising that a robust accumulation of CIZ1 appeared so quickly; this is difficult to reconcile with XIST RNA inducing CIZ1 expression

(D) Active transcription is ongoing even when sparse XIST transcripts paint the chromosome.
(E) Scored in parallel cultures as in (A), few cells exhibit complete silencing (off) by day 3, but at days 5 and 7 these genes are now silenced in many cells.
(F and G) A large dense DNA body lacking CoT-1 RNA (arrow) formed by 3 days is often still associated with an expressed transcription focus (APP).
(H) Active gene transcription on inactivating chr21 with CoT-1 hole, compacted XIST RNA paint, and condensed Barr body.
(I) Genes remain expressed in region of lower-density XIST RNA.
DNA (DAPI) is in blue. Error bars denote SD from the mean. See STAR Methods for information on replicates. Scale bars, 5 μm.

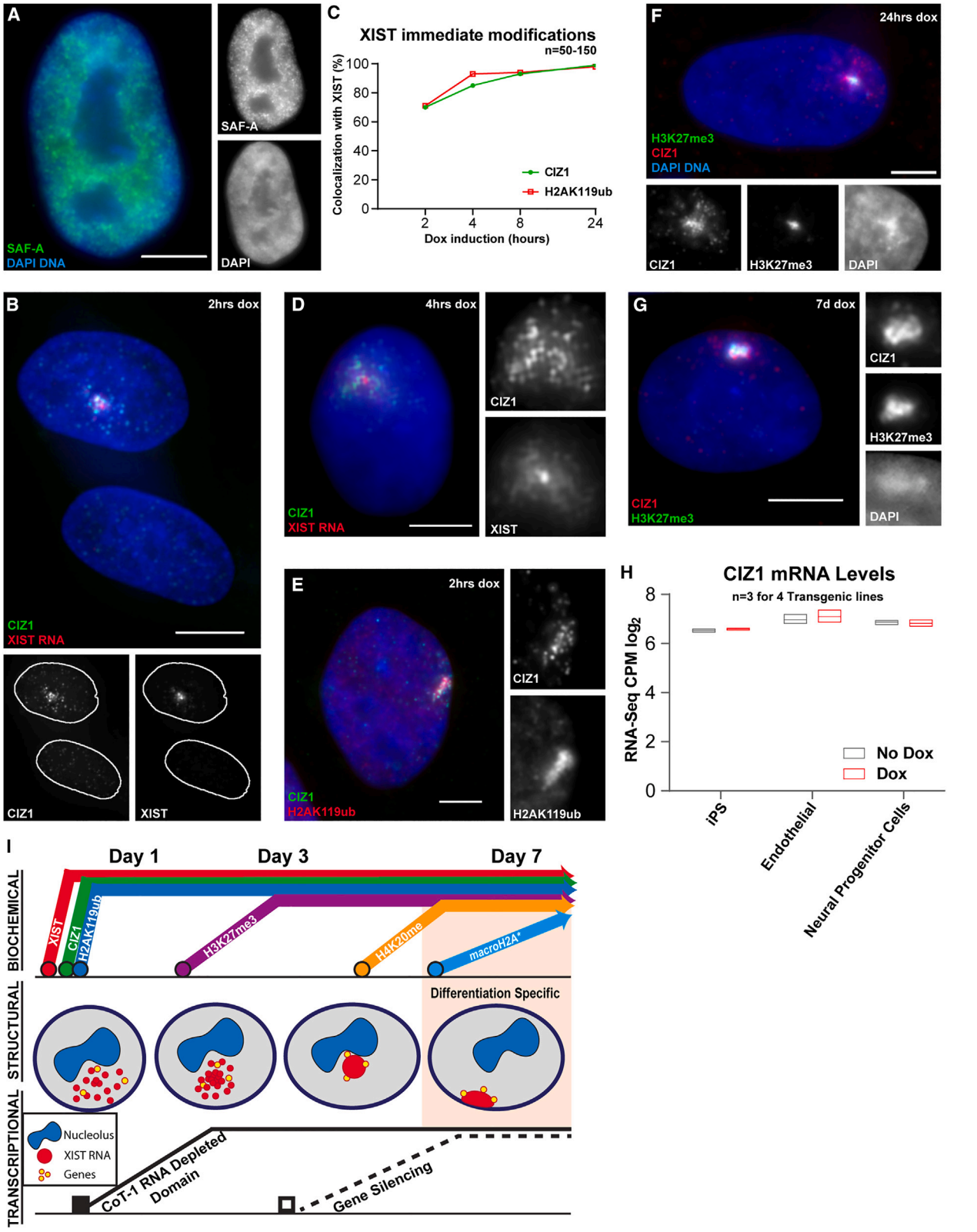

(legend on next page)

and recruiting newly synthesized protein to the chromosome. Supporting this, RNA-seq data from our iPSCs and endothelial and neural derivatives[21] shows CIZ1 mRNA clearly expressed in iPSCs irrespective of XIST induction, and only modestly higher in differentiated cells (Figure 4H). Additionally, earlier studies showed that CIZ1 binds DNA[49] and is present broadly in nuclei but only detectable by immunofluorescence (IF) (with two antibodies) after chromatin removal via a matrix protocol[50]; hence, it was concluded that the CIZ1 epitope is masked by interaction with DNA.[47,51] Thus, we suggest that rather than XIST RNA recruiting CIZ1, CIZ1 is already present, but the epitope detected by a monoclonal antibody to the zinc finger region (DNA-binding domain) is masked in pluripotent cells, except when interacting with XIST RNA.

This concept that XIST RNA likely modifies and reveals a CIZ1 epitope *in situ* is reinforced by findings with SAF-A from the Fackelmayer lab, and recently our lab; SAF-A is enriched with XIST RNA on the Xi, but SAF-A is masked specifically on Xi unless an epitope is revealed by nuclear matrix fractionation, antigen retrieval methods, or a GFP tag.[6,46,52] Interestingly, XIST RNA does not itself bind and directly modify histones, but the RNA does bind these scaffold/matrix proteins, which have both RNA- and DNA-binding domains.[46,47] Thus, XIST may directly impact the nuclear scaffold, altering the architecture of the DNA/RNA territory.

Figure 4I summarizes the above findings on full-length human XIST RNA and highlights a larger theme: within 2 h XIST RNA spreads widely at low levels, immediately impacts certain histone and non-histone chromosomal proteins, and remodels architecture well before chromosome-wide silencing of many protein-coding genes. While we saw few differences with differentiating cells, Figures S5F–S5H summarize that peripheral lamina association was only seen after differentiation (for chr21 or X-chr in human ESCs); hence, we suggest that peripheral lamina localization may be important for this stable state but is not required for gene silencing.

Dense RNA foci of just the small A-repeat domain can silence transcription of local endogenous genes

We further investigated a small domain of XIST with surprising and important findings, which also suggest an explanation for why gene silencing lags architectural condensation. Numerous mESC studies show that deletion of the A-repeat disrupts gene silencing function of this long RNA.[25,53,54] While the A-repeat is clearly required, here we investigate the reciprocal question: might the tiny (450 bp) A-repeat itself be sufficient to repress endogenous loci in *cis*? One previous study examined this in human HT1080 fibrosarcoma cells using qRT-PCR and found that A-repeat RNA could partially repress the GFP reporter on the same plasmid, but, importantly, could not significantly repress even immediately proximal endogenous loci (100 kb to 3 Mb away).[29] Hence, it was concluded that sequences within the missing 96% of full-length XIST RNA are required. Since silencing by XIST is substantially compromised in HT1080 cells,[29,43] we investigated this question further in the iPSC developmental context, where XIST function is optimal. We employed the same inducible promoter, insertion site, and iPSCs (Figure 5A) as for full-length (14 kb) *XIST* (*flXIST*)[19] engineering an inducible 450-bp A-repeat "minigene," and isolated two clones (with similar findings for both). A red fluorescent protein (RFP) gene under EF1α promoter was included downstream of A-repeat, and correct insertion (into chr21 DYRK1A intron) was confirmed by two-color FISH (Figure 5B) and PCR (Figure S6A).

Considering it was not examined previously, A-repeat RNA distribution was of interest. The A-repeat minigene produced a much smaller but intense RNA accumulation (Figure 5C), which occupies an area covering just ~4%–5% of the flXIST RNA territory. Bright focal signal indicates high density of this small sequence at the transcription site, but A-repeat RNA did not spread and localize across the chromosome territory. Induction of A-repeat RNA was able to silence the immediately adjacent RFP reporter under a separate promoter (1.7 kb away), as dox-treated cell colonies lost red fluorescence (Figure 5D), supporting the results of Minks et al.[29] Note that a subset of cells did not lose the RFP, as they did not induce A-repeat RNA due to stochastic silencing of the tet activator (see STAR Methods) (Figures 5D and 5J); this proved useful as an internal negative control (see below).

RFP and A-repeat transgenes are adjacent on the plasmid, but a distinct question is whether the 450-bp transcript, expressed from the DYRK1A intron, can repress that gene's endogenous promoter 90 kb away, and potentially other nearby endogenous loci (see map in Figure S6B). This was evaluated using RNA/RNA FISH to visualize allele-specific TFs. Uninduced cultures show three DYRK1A RNA foci in essentially all cells, affirming that insertion into the intron does not affect DYRK1A transcription (Figure 5B). Eight days after dox induction, the DYRK1A allele in *cis* with A-repeat was silenced in 83% of cells (Figures 5E, 5G, and S6C), whereas RNA foci from the other two alleles remained. For the tandem RFP reporter (or GFP in Minks et al.[29]), it is more difficult to rule out that transcription effects are via steric hindrance, but the DYRK1A promoter is 90 kb away. Furthermore, bright RFP TFs (in uninduced cells), produced from the same site, had no repressive effect on DYRK1A (Figure 5B), providing the initial evidence that the small A-repeat RNA can silence an endogenous locus.

Figure 4. XIST RNA interacts with scaffold factors and rapidly impacts CIZ1

(A and B) Scaffold/matrix protein SAF-A is detected by IF throughout nuclear chromatin in uninduced iPSCs, whereas CIZ1 is only detected when XIST RNA is present.

(C–E) In just 2 h sparse XIST transcripts trigger IF for CIZ1 and H2AK119ub across a large sparse zone.

(F and G) Co-IF showing CIZ1 detected across the initially distended sparse RNA zone, whereas H3K27me3 accumulates in the expanding dense zone.

(H) XIST RNA expression has no effect on CIZ1 mRNA levels.

(I) Schematic summary of results indicating the relative temporal order of changes triggered by human XIST RNA on inactivating chromosome (times are approximate).

DNA (DAPI) is in blue. Error bars denote SD from the mean. See STAR Methods for information on replicates. Scale bars, 5 μm.

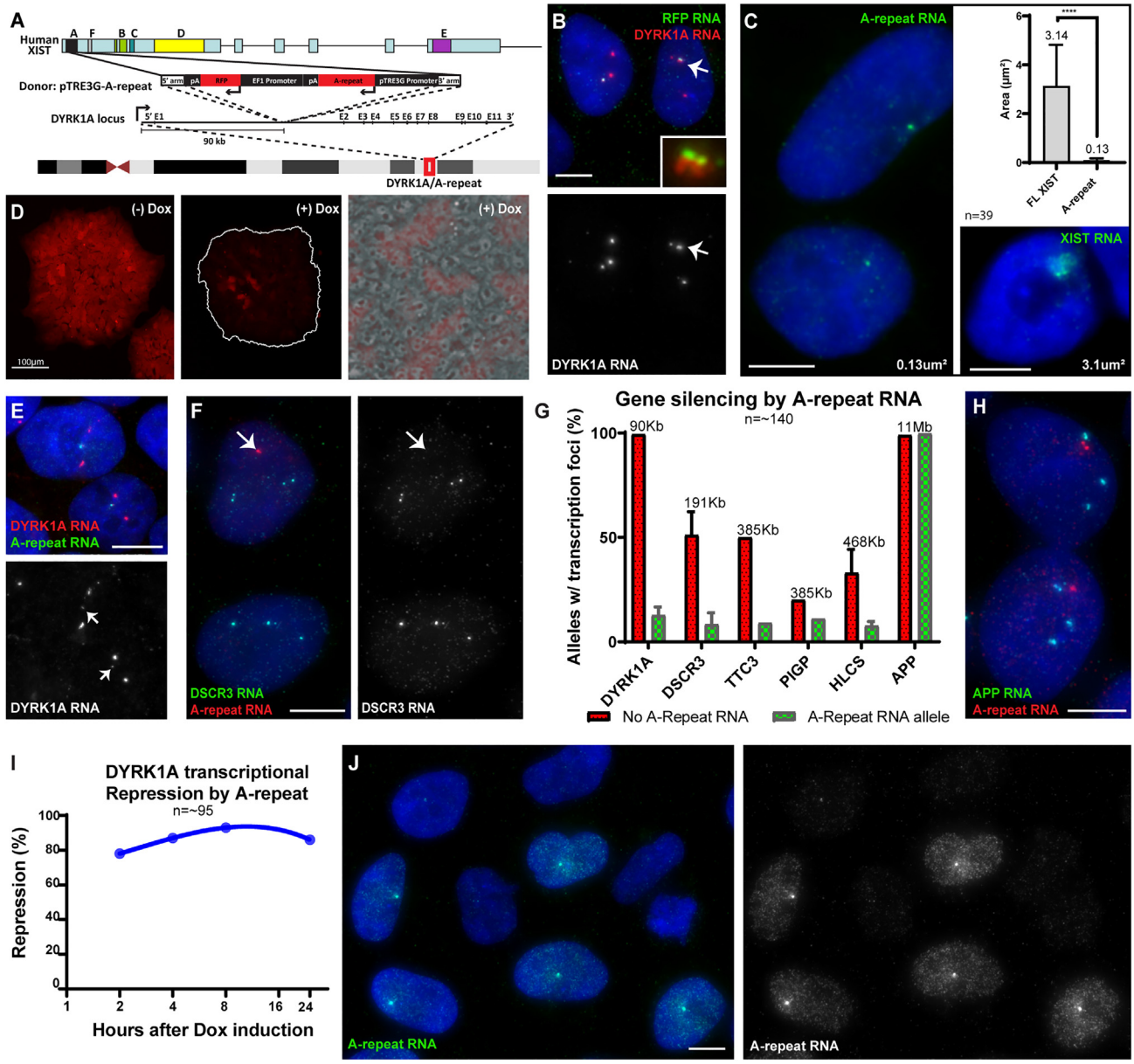

Figure 5. Small dense RNA foci of A-repeat domain can silence transcription of several neighboring endogenous loci

(A) Transgene with human XIST A-repeat under dox inducible promoter and RFP under constitutive promoter, inserted into chr21 DYRK1A intron.

(B) Transcription focus (TF) of RFP transgene colocalizes with TF of one DYRK1A allele.

(C) A-repeat RNA forms small bright focal accumulations and does not spread like XIST RNA (graph of signal areas). Signal difference was significant by unpaired t test.

(D) RFP expression drops after induction of A-repeat RNA. Note that some cells do not respond to dox.

(E–H) A-repeat RNA represses nearby gene alleles in *cis* (e.g., arrows DYRK1A [E] and DSCR3 [F]), but does not repress more distal APP locus (H).

(I) Fraction of nuclei with undetectable/diminished DYRK1A TF in *cis* with A-repeat, compared with the other two alleles.

(J) A-repeat transcripts disperse across the nucleus at significant levels in many cells.

DNA (DAPI) in blue. Error bars denote SD from the mean. See STAR Methods for information on replicates. Scale bars represent 5 µm unless otherwise indicated.

Therefore, we generated genomic probes for two nearby expressed genes further from the integration site, DSCR3 (191 kb away) and TTC3 (385 kb away) (Figure S6B). Since TF strength varies (with, e.g., gene size and intron content), we first quantified detection efficiencies (see STAR Methods and Figures S6D, S6E, and S6I), which were 59% and 50% for DSCR3 and TTC3, respectively (Figure 5G). Dox-induced samples showed TFs at the A-repeat associated allele (Figures 5F, 5G, and S6E), dropping by 82% for DSCR3 and 83% for TTC3. Given these surprising results, we examined two other nearby expressed genes, PIG1

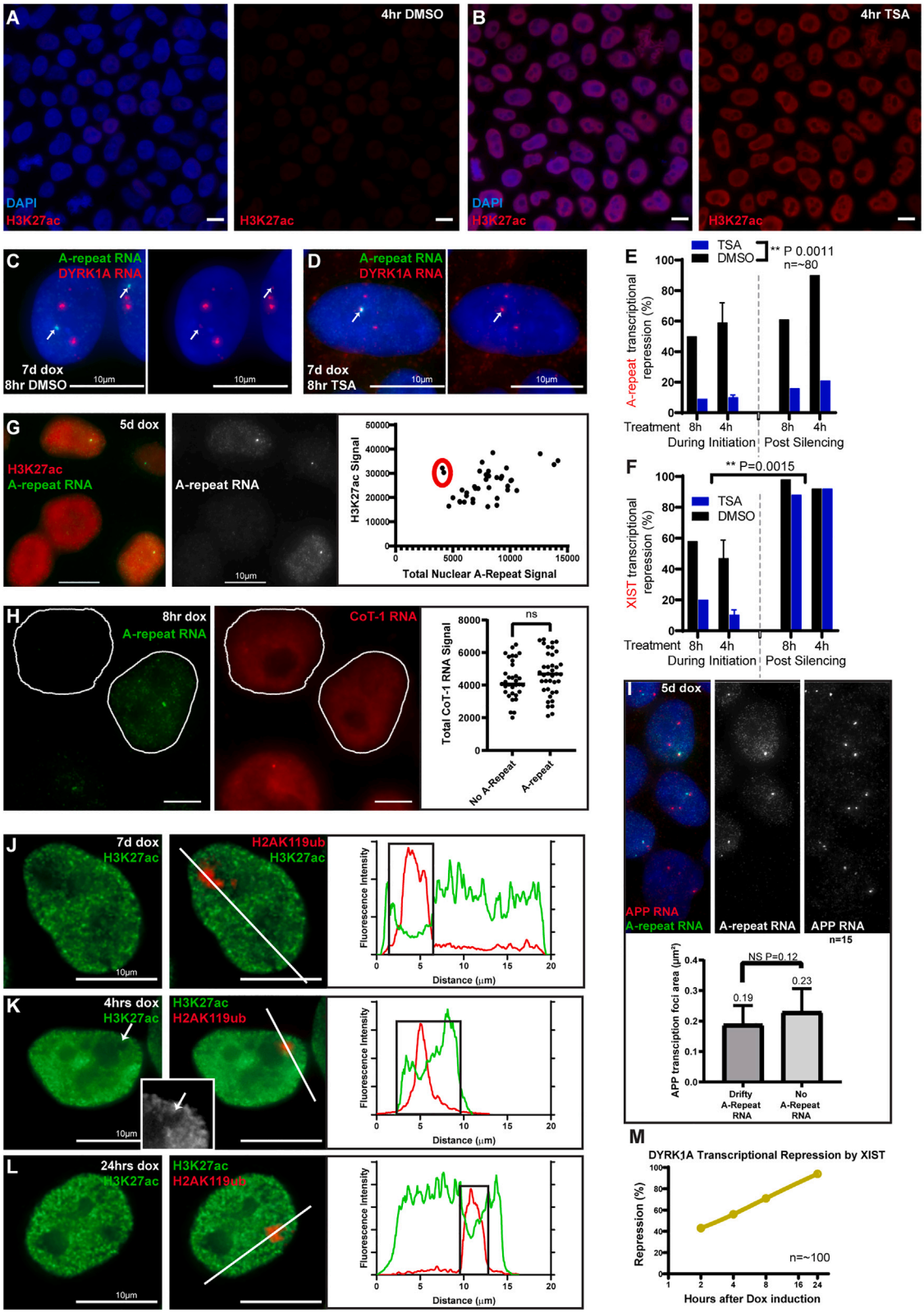

(legend on next page)

(385 kb away) and HLCS (468 kb away) for which detection efficiency was somewhat lower (Figures S6F and S6G) but, nonetheless, upon induction, TFs at the A-repeat allele dropped ~46% and 74%, respectively (Figure 5G). While silencing efficiency may decline across this distance, gene silencing still occurred in many cells for loci a few hundred kilobases from the insertion site. We also examined a more distal gene, APP (11 Mb away), and in this case three TFs were always detected after inducing the A-repeat, with no reduction in size or intensity of RNA from the allele nearest the A-repeat RNA (Figures 5G, 5H, and S6H).

We conclude that, in developmentally appropriate cells, the A-repeat fragment alone can silence transcription of endogenous genes, limited to the "local chromosomal neighborhood" of the dense RNA foci (shown here for a region ~500 kb) with no effect on a distant locus. Surprisingly, this tiny 450-bp fragment retains this functionality without 96% of the XIST transcript.

A few other observations are relevant to other findings discussed below. First, since A-repeat transcripts do not spread, a focal concentration may form and silence genes rapidly. Hence, we examined cells induced for 2 h and found that bright A-repeat RNA foci had formed and repressed the DYRK1A allele (Figure 5I). Thus, these dense RNA foci can very quickly silence nearby gene transcription. Second, many cells had dense RNA foci and visible transcripts dispersed throughout the nucleoplasm (Figure 5J). Unlike RFP mRNA, A-repeat RNA is not detected in the cytoplasm and thus may not be exported (Figures S6J and S6K). With transcriptional inhibition, A-repeat RNA foci are gone by 30 min, whereas nucleoplasmic signal becomes undetectable after an hour (Figures S6L and S6M). Hence, newly synthesized A-repeat transcripts accumulate briefly in dense RNA foci that can repress nearby genes, but otherwise these transcripts are free to disperse through the nucleus.

Dense A-repeat RNA and continual histone deacetylase activity are required to initiate and maintain gene silencing

The aforesaid results show that the A-repeat RNA itself can silence genes and can do so rapidly. Since flXIST RNA contains the A-repeat and spreads widely within hours, why does it not silence genes quickly (Figure 3I)? The sparse flXIST RNA clearly modifies H2A and CIZ1 within just 2 h, yet it took days to silence the genes examined, and this occurred only after RNA territory coalescence.

To gain insight into this conundrum, we considered how the A-repeat functions. The A-repeat region in flXIST has been implicated in histone deacetylation and chromosome organization with the nuclear lamina. Several studies support that the A-repeat in flXIST recruits histone deacetylases (HDACs) for H3K27 deacetylation via SPEN, which is important for the chromosome silencing process.[22,24,36,38,55] It was also reported that the A-repeat region binds the lamin B receptor (LBR),[55] which is thought to tether the chromosome to the peripheral lamina in a manner required for gene silencing.[56] However, as noted above, in our system chromosome silencing by flXIST occurs without movement to the peripheral lamina in pluripotent cells (see Figure S5F). Furthermore, A-repeat RNA foci do not move to the periphery in pluripotent or differentiated cells (Figure S7A) but still repress genes locally (e.g., Figure 5G).

Hence, we focused on whether this 450-bp fragment acts via histone deacetylation, using trichostatin A (TSA) inhibition of HDACs. Just a 4-h TSA treatment rapidly increases H3K27ac across the nucleus (Figures 6A and 6B). The fact that histone reacetylation occurs so quickly illuminates the dynamic nature of the ongoing balance between histone acetylation/deacetylation, a point important for findings below and our model described in the discussion. TSA treatment of iPSCs, started concomitantly with dox induction, clearly prevented gene silencing (Figures 6E and S7B); thus, this isolated RNA fragment still functions via histone deacetylation. Importantly, if TSA was added days after inducing A-repeat RNA the gene became expressed, demonstrating that continual HDAC activity was required to maintain gene silencing; this defines an "HDAC-dependent" state (Figures 6C–6E and S7C). A fundamental difference is seen with flXIST RNA (Figures 6F, S7D, and S7E) where HDAC activity is required to initiate gene silencing but not to maintain it. This defines an "HDAC-independent" state, indicating that other modifications by flXIST RNA block reacetylation, such as subsequent methylation of the same H3K27 residue. Note that this is distinct from the "XIST-independent silent state" that occurs only after differentiation.

Our ability to examine A-repeat function apart from other XIST effects reveals that the required A-repeat-dependent step is not a stable epigenetic change but a highly dynamic and reversible one. Unlike stable epigenomic changes, transcriptional modulation depends on the balance between histone acetylation and deacetylation,[57,58] which will depend on the local concentration of factors involved in these countervailing processes. In light of this, we further considered how A-repeat RNA density likely impacts this balance by examining the many cells noted above that contain lower levels of A-repeat RNA across the nucleoplasm

Figure 6. Gene silencing requires effective histone deacetylation and depends on high local density of A-repeat RNA

(A and B) Nuclear H3K27ac markedly increases with just a 4-h 10 μM TSA inhibition of HDACs, compared with DMSO-treated controls.

(C–E) HDAC inhibition impairs A-repeat RNA-mediated transcriptional repression of DYRK1A gene during both initiation of silencing (simultaneous dox and 5–10 μM TSA) and after silencing is established by 7 days of dox (significant by two-way ANOVA). Panels on right (C and D) have A-repeat signal removed to show gene TF (arrows in C and D indicate transgenic locus).

(F) HDAC inhibition impairs XIST RNA-mediated gene silencing (DYRK1A) only during initiation of silencing but not after silencing has been established (APP). Initiation vs Post Silencing groups were significantly different by two-way ANOVA.

(G–I) Readily detectable but lower levels of dispersed A-repeat RNA had no discernible effect on nuclear levels for H3K27ac (G), nor CoT-1 RNA levels (H) or specific gene TFs (I) when compared with adjacent cells lacking A-repeat expression. Cells lacking A-repeat RNA in (G) are circled in red in the graph. Unpaired t-test shows no significant difference (ns) in graphs (H and I).

(J–L) A prominent "hole" in the nucleoplasmic H3K27ac signal encompasses the entire H2AK119ub territory in cells with silenced chromosome (shown for 7 days post induction) (J), while a smaller "dip" in the H3K27ac signal is seen primarily at the center of the H2AK119ub territory at earlier time points (K and L).

(M) Full-length XIST RNA can repress the adjacent (90 kb away) DYRK1A promoter within hours.

DNA (DAPI) in blue. Error bars denote SD from the mean. See STAR Methods for information on replicates. Scale bars represent 5 μm unless otherwise indicated.

(in addition to dense RNA foci). Comparing these cells directly with neighboring cells that lack any A-repeat expression allowed us to examine whether lower but significant levels of A-repeat RNA had a detectable effect on nuclear H3K27acetylation levels, specific gene TFs, or CoT-1 RNA. Based on visual inspection as well as microfluorimetric analysis, cells with substantial dispersed A-repeat RNA had no discernible reduction in H3K27ac (Figure 6G) or CoT-1 RNA intensity levels (Figures 6H and S7F). Figure 6I illustrates that the two other alleles in nuclei with substantial dispersed A-repeat RNA show no diminution relative to adjacent control cells. This is reinforced from the above analysis of specific genes, in which only TFs from A-repeat linked alleles were repressed.

Finally, costaining for H3K27ac and H2AK119ub further supports that histone deacetylation appears more slowly and density limited than ubiquitination. On a fully silenced chromosome, the loss of H3K27ac creates a prominent dark "acetylation void" over the chromosome (Figure 6J). However, during early hours, when H2AK119ub is bright across the large sparse territory, chromosome-wide decrease in histone acetylation is barely discernible by IF, although a dip in acetylation is evident over the small dense RNA zone, seen in all of the 25 cells scored (Figures 6K [inset] and 6L). Consistent with this, we tested the DYRK1A gene, which occupies an unusual location at the dense epicenter of flXIST expression, and found that it is repressed more rapidly than the genes tested above (Figure 6M).

Understanding these properties of A-repeat RNA function is itself significant, but findings also suggest a plausible explanation for a central point shown for flXIST RNA: that it acts to compact the DNA territory, and thus build RNA density, before chromosome-wide silencing of actively expressed genes.

DISCUSSION

This study provides significant findings regarding steps in whole-chromosome silencing by human XIST RNA, and in addition demonstrates surprising and impactful results regarding the A-repeat minigene. The unanticipated finding that a tiny XIST fragment can silence gene transcription has translational implications, such as for Down syndrome and small duplication disorders, and this important aspect is the subject of ongoing studies and will be discussed elsewhere. Here we focus on how findings with the A-repeat XIST minigene informs understanding of the function of full-length XIST RNA. Based on our collective results, we will propose a model whereby XIST RNA acts early to condense chromosome architecture to build RNA density which facilitates, rather than just reflects, initiation of chromosome-wide silencing of actively expressed genes.

XIST RNA induces a condensed Barr body before chromosome-wide gene silencing

The inducible XIST iPSC system made it possible to investigate, with high temporal and spatial resolution, changes triggered by human XIST RNA on active chromosome territories as they undergo comprehensive silencing and condensation. As summarized in Figure 4I, H4K20 and macroH2A modifications are induced a day or more after H3K27me3 and H2AK119ub. Interestingly, kinetics was similar in pluripotent and differentiating cells except for macroH2A, which is seen primarily post differentiation. H2AK119ub is seen at the earliest time point examined (2 h), several hours before H3K27me3, supporting (for human XIST) a debated point in mice that PRC1 acts before PRC2.[59]

Key findings came from scrutiny of early XIST RNA distribution within nuclear structure and the highly decondensed chromatin of stem cells. Sensitive *in situ* analysis shows that barely detectable XIST transcripts rapidly spread across a large but defined nuclear territory, the "sparse zone," encompassing the initially small "dense zone." This sparse RNA is seen at early time points, and its detection requires optimal conditions for RNA FISH and imaging analysis. A pivotal point is that these rapidly spreading transcripts are not inconsequential drift: they immediately trigger robust H2AK119ub and CIZ1 staining across the large sparse RNA zone.

This led to another finding and concept: that the cytological density of XIST RNA is a factor that can impact on whether a particular modification is induced in that region. Here we assay and show significance for the cytological RNA distribution in the nuclear territory, distinct from distributions on the linear DNA sequence, as in RNA-immunoprecipitation-based or chromatin immunoprecipitation (ChIP)-based assays. Some changes are clearly induced by very sparse transcripts whereas others are only seen at sites of high RNA density, as summarized in Figure 7A. H3K27me3 stained brightly in the dense zone but not in the large sparse zone intensely stained for CIZ1 or H2AK119ub. The assay for deacetylation (loss of H3K27ac staining) is inherently less sensitive. However, we can conclude that loss of H3K27ac in the early time points is more limited and mostly evident in the dense zone; this fits with other evidence given below that stable H3K27 deacetylation requires higher RNA density (than H2AK119ub and CIZ1 modifications).

Delayed gene silencing by XIST may help explain biallelic "dampening" in human IVF embryos

A central point shown is that XIST RNA largely condenses architecture by day 1, yet silencing of several broadly mapped genes is not seen until day 3 and not complete until days later. Of note, an early study of endogenous X-inactivation in female mESCs also found that gene silencing took a few days and occurred after formation of the CoT-1 RNA and RNA polymerase II exclusion domain.[23] Timing of gene silencing likely varies somewhat between studies, model systems, and possibly species. However, many studies using RNA-seq and ChIP on averaged populations do not examine architecture and cannot address its relative timing to gene silencing. Other studies have found a significant delay between XIST RNA expression and full gene silencing.[22] Of particular interest, observations in human IVF embryos have noted transient uncoupling between XIST RNA spread and X-inactivation, which is reminiscent of the lag in gene silencing we report here. In cultured embryos many cells express XIST RNA from both X chromosomes yet neither is initially fully silenced, although transcriptional "dampening" is seen. Subsequently, biallelic expression is lost and XIST RNA fully silences one X chromosome.[60] Our results showing early repression of the DYRK1A gene (near the XIST

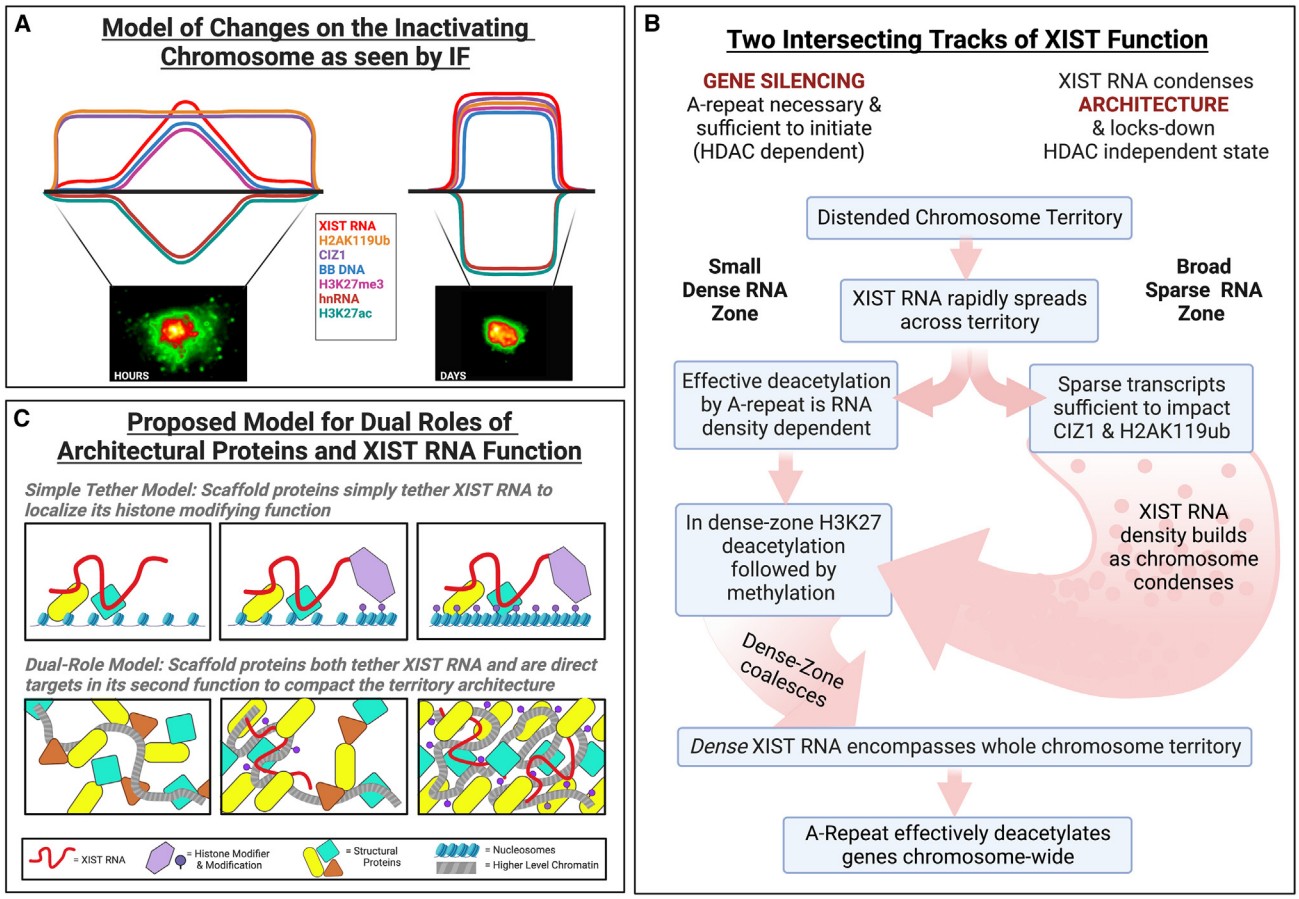

Figure 7. Models of XIST RNA function based on collective results

(A) Idealized summary diagram for relative distributions of XIST RNA and other changes on the inactivating chromosome, as observed here *in situ*. Left, early hours of chromosome silencing and right, after the process is more complete. Early in the process, XIST RNA is very unevenly distributed, in a large sparse zone and smaller dense zone. Some steps are density dependent (V-shaped profiles early in the process) and others are not (low flat profiles early). Distribution becomes more uniform after condensation of the DNA/RNA territory.

(B) Model for two-intersecting tracks of XIST RNA function. The flow chart incorporates findings and concepts (detailed in text) supporting a model whereby XIST RNA function includes early and direct impact on territory architecture, distinct from histone modifications which repress local gene transcription. The model further proposes that condensation of the distended chromosome and coalescence of the dense RNA territory facilitates density-dependent A-repeat function required to silence active genes and initiate the histone cascade.

(C) Models for the role of scaffold proteins in XIST RNA function. Simple tether model (top): matrix/scaffold proteins (e.g., CIZ1, SAF-A) are thought to function by simply tethering XIST RNA to localize the RNA's function in recruiting histone-modifying enzymes, triggering a histone cascade that silences genes and condenses the chromosome. Proposed dual-role model (bottom): here we suggest that scaffold proteins both tether XIST RNA and are direct targets in its second function; the RNA interacts with and impacts the arrangement of non-histone proteins in a territory scaffold, promoting cytological-scale condensation. In addition, XIST RNA triggers local histone modifications important for gene silencing, which may further contribute to architectural condensation. Figures created with BioRender.com.

locus) and decreased CoT-1 RNA may be analogous to transcriptional "dampening" in IVF embryos. Since silencing both X chromosomes would be strongly selected against, a few days' lag-time before chromosome-wide silencing would likely create a transient period permissive to biallelic XIST expression. After this, feedback regulation or selection would assure that only one chromosome is silenced, even if XIST transcription may be "promiscuous." While we have studied a monoallelic transgenic system, a lag in human chromosome silencing occurs in both systems and may reflect the natural biology of XIST function. Results suggest that this lag-time allows for changes that condense the chromosome and build a dense RNA accumulation, which then facilitates chromosome-wide silencing, further explained below.

Compaction builds RNA density, which facilitates an unstable step required to initiate full epigenetic silencing

We demonstrate that A-repeat RNA does not spread and localize on the chromosome but accumulates in small bright RNA foci, which, remarkably, can silence local gene transcription and do so rapidly. Since A-repeat transcripts are sufficient to silence transcription in 2–4 h, why don't sparse XIST transcripts that spread rapidly (and induce H2AK119ub and CIZ1) also silence active

genes in hours rather than days? Findings indicate that sufficiently high local density of A-repeat RNA is required to achieve effective H3K27 deacetylation in active chromatin regions.

Multiple observations indicate that gene silencing by the A-repeat RNA is density limited. Only genes/alleles at or near the site of dense RNA foci are repressed; even when substantial dispersed nucleoplasmic A-repeat RNA was clearly visible, it had no discernible impact on H3K27ac levels, gene TFs, or CoT-1 RNA levels. Similarly, sparse-zone XIST transcripts do not rapidly silence most genes. A key to understanding why XIST RNA cytological density is initially limiting derives from the demonstration that A-repeat RNA requires HDAC activity to initiate silencing, and requires continuous HDAC activity to maintain gene silencing. Importantly, transcriptional modulation by histone acetylation/deacetylation is not a stable epigenetic regulation but an ongoing dynamic balance between histone acetyltransferase and HDAC activities in a local region.[57,58] The transient nature of this is evidenced by how quickly just 4 h of HDAC inhibition dramatically increases nuclear H3K27 acetylation (Figure 6B). We suggest it is pivotal for understanding the connection between architecture and gene silencing that this required step to initiate stable gene silencing is itself a highly unstable, non-epigenetic step.

Given this, it is logical that effective histone deacetylation requires sufficiently high RNA density to recruit deacetylase activity via Spen[54] that is sufficient to overcome acetylase activity in active regions. Active genes cluster in nuclear "hubs,"[8,31] and we suggest that creating a hub of inactivity (i.e., a silent Barr body) may facilitate silencing by favoring deacetylation over acetylation. Hence, chromosome condensation may precede silencing of many genes because it creates an RNA-dense compartment that favors effective histone deacetylation over acetylation.

While not detailed here, other XIST domains must then be required to lock down an "HDAC-independent state"; we suggest that methylation of the same H3K27 residue, once it is deacetylated, potentially blocks reacetylation.

XIST RNA may condense the territory by directly impacting architectural factors

This study highlights that XIST RNA function involves not only silencing of protein-coding genes but dramatic changes to large-scale territory architecture. Figure 7B proposes a model whereby XIST function involves two distinct but inter-related tracks: one that involves histone modifications to impact local nucleosome structure (e.g., histone deacetylation) and another that acts early to modify elements of large-scale territory architecture (e.g., CIZ1, SAF-A). While histone modifications have been heavily studied, the possible role of nuclear matrix/scaffold proteins, not just as tethers but as targets of XIST function, has been less explored. Both CIZ1 and SAF-A have DNA- and RNA-binding domains thought to localize XIST RNA for its histone-modifying functions (Figure 7C); however, we propose an alternative concept for the role of CIZ1 or SAF-A, not as simply tethers for RNA but also as targets of XIST RNA. The immediacy with which XIST RNA triggers staining for CIZ1, together with the known masking of CIZ1 epitopes by interaction with DNA,[51] strongly suggests that XIST triggers a conformational change in CIZ1. We suggest that XIST RNA directly impacts the arrangement of one or more scaffold proteins and thereby modifies and condenses cytological-scale territory architecture (Figure 7C). This may prove key to what we envision is the "architectural track" of XIST function that impacts cytological-scale structure, as distinct from local changes to nucleosomal histones (Figure 7B).

The chromosome inactivation process must also be understood in terms of a chromosome that is overwhelmingly non-coding DNA. The Barr body is rich in repetitive sequences and, even in fully silenced chromosomes, we showed that 14 protein-coding genes examined localized primarily at the outer edge of this dense mass of DNA.[5,44] Hence, the repeat-rich non-coding DNA may play a role in forming a repressive compartment. Relevant to this idea are ChIP-based findings that XIST RNA first induces H2AK119 and H3K27 modifications in intergenic sequences and less active regions, before active genes[22,36]; this fits well with the model proposed here that modifications may initially condense the large territory comprised largely of non-coding DNA before silencing protein-coding genes.

Related to the role of non-coding DNA, results of this study and others from our lab[5,6,45,52] point to the potential biological import of repeat-rich "junk" RNA (CoT-1 RNA), comprised primarily of introns of pre-mRNA and many thousands of low-level lncRNAs. We have shown that euchromatin-associated CoT-1 hnRNAs platform an insoluble RNP scaffold (with matrix proteins such as SAF-A) that counters chromosome condensation.[6] Since XIST RNA is strictly and inversely correlated with CoT-1 RNA[45] and removal of CoT-1 hnRNA rapidly causes chromatin condensation, XIST RNA may promote chromosome condensation in part by displacing or repressing CoT-1 RNAs and the RNP scaffold that counters condensation.[6] However, compaction of the chromosome likely also involves phase separation of RNP scaffold factors that form multivalent interactions and coalesce with greater RNA density, as also recently shown for Spen and XIST RNA.[61,62] We envision that future studies will illuminate how XIST RNA impacts RNP scaffold factors in addition to modifying histones.

Limitations of the study

The experimental system made it possible to examine very early steps triggered by human XIST RNA in the direct context of changing architecture. XIST RNA has been shown to stably silence all genes across the trisomic chr21; however, we cannot rule out that there is any difference in the process for an autosome. For example, the X chromosome has abundant, more uniformly distributed LINE1 elements, which might somehow influence kinetics of changes. Nonetheless, the relative order of changes demonstrated here are valid for the process whereby human XIST RNA fully functions to silence the human chromosome. As is true for mouse Xist studies, our system does not model biallelic XIST expression seen in cultured human IVF embryos. However, both systems show a lag between XIST RNA spread and chromosome-wide gene silencing, which lends credibility that findings modeled in our system may reflect the *in vivo* process. The approach here provides insights into how XIST functions in the structural context in which it occurs, although a limitation is that it does not provide genomic sequence information. We have cited ChIP studies which show early effects of XIST RNA on intergenic chromatin, consistent

with our model of early condensation of a largely non-coding chromosome. The number of genes examined here is limited, and a time course of RNA-seq would more fully define gene silencing kinetics in human cells. Full understanding of XIST function will require complementary approaches to interconnect the chromosome territory (and its architecture) with the linear DNA sequence.

STAR★METHODS

Detailed methods are provided in the online version of this paper and include the following:

- KEY RESOURCES TABLE
- RESOURCE AVAILABILITY
  - Lead contact
  - Materials availability
  - Data and code availability
- EXPERIMENTAL MODEL AND SUBJECT DETAILS
  - Human cells
  - Mouse cells
- METHOD DETAILS
  - pTRE3G-A-repeat-EF1a-RFP::DYRK1A plasmid
  - DNA and RNA FISH and immunostaining
- QUANTIFICATION AND STATISTICAL ANALYSIS
  - Image analysis

SUPPLEMENTAL INFORMATION

Supplemental information can be found online at https://doi.org/10.1016/j.celrep.2023.112686.

ACKNOWLEDGMENTS

We appreciate funding from NIH grants R01HD094788, R35GM122597, and R01HD091357 to J.B.L. M.V. received additional support from F32 AG056131-01. We thank Lawrence lab members for their support throughout this study, particularly Yuanchun Jing for technical assistance, Jennifer Moon for sharing RNA-seq data for CIZ1, and Kelly Smith for thoughtful comments on the manuscript.

AUTHOR CONTRIBUTIONS

M.V. and M.B. engineered constructs and cell lines and conducted experiments on XIST, A-repeat, gene silencing, and chromosome modifications; D.M.C. and B.D. conducted experiments on full-length XIST RNA; M.V., M.B., L.L.H. and J.B.L. analyzed results; J.B.L., L.L.H., M.V., and M.B. designed the experiments and wrote the manuscript.

DECLARATION OF INTERESTS

J.B.L., M.V., and M.B. are inventors on a patent application arising from aspects of this work.

Received: February 24, 2021
Revised: October 31, 2022
Accepted: June 8, 2023
Published: June 28, 2023

REFERENCES

1. Dixon-McDougall, T., and Brown, C. (2016). The making of a Barr body: the mosaic of factors that eXIST on the mammalian inactive X chromosome. Biochem. Cell. Biol. *94*, 56–70. https://doi.org/10.1139/bcb-2015-0016.
2. Strehle, M., and Guttman, M. (2020). Xist drives spatial compartmentalization of DNA and protein to orchestrate initiation and maintenance of X inactivation. Curr. Opin. Cell Biol. *64*, 139–147. https://doi.org/10.1016/j.ceb.2020.04.009.
3. Creamer, K.M., and Lawrence, J.B. (2017). Xist RNA: a window into the broader role of RNA in nuclear chromosome architecture. Philos. Trans. R. Soc. Lond. B Biol. Sci. *372*, 20160360. https://doi.org/10.1098/rstb.2016.0360.
4. Hall, L.L., and Lawrence, J.B. (2016). RNA as a fundamental component of interphase chromosomes: could repeats prove key? Curr. Opin. Genet. Dev. *37*, 137–147. https://doi.org/10.1016/j.gde.2016.04.005.
5. Hall, L.L., and Lawrence, J.B. (2010). XIST RNA and architecture of the inactive X chromosome: implications for the repeat genome. Cold Spring Harbor Symp. Quant. Biol. *75*, 345–356. https://doi.org/10.1101/sqb.2010.75.030.
6. Creamer, K.M., Kolpa, H.J., and Lawrence, J.B. (2021). Nascent RNA scaffolds contribute to chromosome territory architecture and counter chromatin compaction. Mol. Cell. *81*, 3509–3525.e5. https://doi.org/10.1016/j.molcel.2021.07.004.
7. Bickmore, W.A. (2013). The spatial organization of the human genome. Annu. Rev. Genom. Hum. Genet. *14*, 67–84. https://doi.org/10.1146/annurev-genom-091212-153515.
8. Smith, K.P., Hall, L.L., and Lawrence, J.B. (2020). Nuclear hubs built on RNAs and clustered organization of the genome. Curr. Opin. Cell Biol. *64*, 67–76. https://doi.org/10.1016/j.ceb.2020.02.015.
9. Chow, J.C., Hall, L.L., Clemson, C.M., Lawrence, J.B., and Brown, C.J. (2003). Characterization of expression at the human XIST locus in somatic, embryonal carcinoma, and transgenic cell lines. Genomics *82*, 309–322.
10. Migeon, B.R. (2017). Choosing the active X: the human version of X inactivation. Trends Genet. *33*, 899–909. https://doi.org/10.1016/j.tig.2017.09.005.
11. Sahakyan, A., Yang, Y., and Plath, K. (2018). The role of xist in X-chromosome dosage compensation. Trends Cell Biol. *28*, 999–1013. https://doi.org/10.1016/j.tcb.2018.05.005.
12. Okamoto, I., Patrat, C., Thépot, D., Peynot, N., Fauque, P., Daniel, N., Diabangouaya, P., Wolf, J.P., Renard, J.P., Duranthon, V., and Heard, E. (2011). Eutherian mammals use diverse strategies to initiate X-chromosome inactivation during development. Nature *472*, 370–374. https://doi.org/10.1038/nature09872.
13. Hoffman, L.M., Hall, L., Batten, J.L., Young, H., Pardasani, D., Baetge, E.E., Lawrence, J., and Carpenter, M.K. (2005). X-inactivation status varies in human embryonic stem cell lines. Stem Cell. *23*, 1468–1478. https://doi.org/10.1634/stemcells.2004-0371.
14. O'Neill, L.P., Randall, T.E., Lavender, J., Spotswood, H.T., Lee, J.T., and Turner, B.M. (2003). X-linked genes in female embryonic stem cells carry an epigenetic mark prior to the onset of X inactivation. Hum. Mol. Genet. *12*, 1783–1790. https://doi.org/10.1093/hmg/ddg193.
15. Tchieu, J., Kuoy, E., Chin, M.H., Trinh, H., Patterson, M., Sherman, S.P., Aimiuwu, O., Lindgren, A., Hakimian, S., Zack, J.A., et al. (2010). Female human iPSCs retain an inactive X chromosome. Cell Stem Cell *7*, 329–342. https://doi.org/10.1016/j.stem.2010.06.024.
16. Diaz Perez, S.V., Kim, R., Li, Z., Marquez, V.E., Patel, S., Plath, K., and Clark, A.T. (2012). Derivation of new human embryonic stem cell lines reveals rapid epigenetic progression in vitro that can be prevented by chemical modification of chromatin. Hum. Mol. Genet. *21*, 751–764. https://doi.org/10.1093/hmg/ddr506.
17. Hall, L.L., Byron, M., Butler, J., Becker, K.A., Nelson, A., Amit, M., Itskovitz-Eldor, J., Stein, J., Stein, G., Ware, C., and Lawrence, J.B. (2008).

X-inactivation reveals epigenetic anomalies in most hESC but identifies sublines that initiate as expected. J. Cell. Physiol. *216*, 445–452. https://doi.org/10.1002/jcp.21411.

18. Sahakyan, A., Kim, R., Chronis, C., Sabri, S., Bonora, G., Theunissen, T.W., Kuoy, E., Langerman, J., Clark, A.T., Jaenisch, R., and Plath, K. (2017). Human naive pluripotent stem cells model X chromosome dampening and X inactivation. Cell Stem Cell *20*, 87–101. https://doi.org/10.1016/j.stem.2016.10.006.

19. Jiang, J., Jing, Y., Cost, G.J., Chiang, J.C., Kolpa, H.J., Cotton, A.M., Carone, D.M., Carone, B.R., Shivak, D.A., Guschin, D.Y., et al. (2013). Translating dosage compensation to trisomy 21. Nature *500*, 296–300. https://doi.org/10.1038/nature12394.

20. Czerminski, J.T., and Lawrence, J.B. (2020). Silencing trisomy 21 with XIST in neural stem cells promotes neuronal differentiation. Dev. Cell *52*, 294–308.e293. https://doi.org/10.1016/j.devcel.2019.12.015.

21. Moon, J.E., and Lawrence, J.B. (2022). Chromosome silencing in vitro reveals trisomy 21 causes cell-autonomous deficits in angiogenesis and early dysregulation in Notch signaling. Cell Rep. *40*, 111174. https://doi.org/10.1016/j.celrep.2022.111174.

22. Nesterova, T.B., Wei, G., Coker, H., Pintacuda, G., Bowness, J.S., Zhang, T., Almeida, M., Bloechl, B., Moindrot, B., Carter, E.J., et al. (2019). Systematic allelic analysis defines the interplay of key pathways in X chromosome inactivation. Nat. Commun. *10*, 3129. https://doi.org/10.1038/s41467-019-11171-3.

23. Chaumeil, J., Le Baccon, P., Wutz, A., and Heard, E. (2006). A novel role for Xist RNA in the formation of a repressive nuclear compartment into which genes are recruited when silenced. Genes Dev. *20*, 2223–2237. https://doi.org/10.1101/gad.380906.

24. Brockdorff, N., Bowness, J.S., and Wei, G. (2020). Progress toward understanding chromosome silencing by Xist RNA. Genes Dev. *34*, 733–744. https://doi.org/10.1101/gad.337196.120.

25. Wutz, A., Rasmussen, T.P., and Jaenisch, R. (2002). Chromosomal silencing and localization are mediated by different domains of Xist RNA. Nat. Genet. *30*, 167–174. https://doi.org/10.1038/ng820.

26. Bousard, A., Raposo, A.C., Żylicz, J.J., Picard, C., Pires, V.B., Qi, Y., Gil, C., Syx, L., Chang, H.Y., Heard, E., and da Rocha, S.T. (2019). The role of Xist-mediated Polycomb recruitment in the initiation of X-chromosome inactivation. EMBO Rep. *20*, e48019. https://doi.org/10.15252/embr.201948019.

27. Ha, N., Lai, L.T., Chelliah, R., Zhen, Y., Yi Vanessa, S.P., Lai, S.K., Li, H.Y., Ludwig, A., Sandin, S., Chen, L., and Zhang, L.F. (2018). Live-cell imaging and functional dissection of xist RNA reveal mechanisms of X chromosome inactivation and reactivation. iScience *8*, 1–14. https://doi.org/10.1016/j.isci.2018.09.007.

28. Colognori, D., Sunwoo, H., Kriz, A.J., Wang, C.Y., and Lee, J.T. (2019). Xist deletional analysis reveals an interdependency between xist RNA and polycomb complexes for spreading along the inactive X. Mol. Cell. *74*, 101–117.e10. https://doi.org/10.1016/j.molcel.2019.01.015.

29. Minks, J., Baldry, S.E., Yang, C., Cotton, A.M., and Brown, C.J. (2013). XIST-induced silencing of flanking genes is achieved by additive action of repeat a monomers in human somatic cells. Epigenet. Chromatin *6*, 23. https://doi.org/10.1186/1756-8935-6-23.

30. Xing, Y., Johnson, C.V., Dobner, P.R., and Lawrence, J.B. (1993). Higher level organization of individual gene transcription and RNA splicing. Science *259*, 1326–1330.

31. Shopland, L.S., Johnson, C.V., Byron, M., McNeil, J., and Lawrence, J.B. (2003). Clustering of multiple specific genes and gene-rich R-bands around SC-35 domains: evidence for local euchromatic neighborhoods. J. Cell Biol. *162*, 981–990. https://doi.org/10.1083/jcb.200303131.

32. Chen, Y., and Belmont, A.S. (2019). Genome organization around nuclear speckles. Curr. Opin. Genet. Dev. *55*, 91–99. https://doi.org/10.1016/j.gde.2019.06.008.

33. Kurz, A., Lampel, S., Nickolenko, J.E., Bradl, J., Benner, A., Zirbel, R.M., Cremer, T., and Lichter, P. (1996). Active and inactive genes localize preferentially in the periphery of chromosome territories. J. Cell Biol. *135*, 1195–1205. https://doi.org/10.1083/jcb.135.5.1195.

34. Smith, K.P., Moen, P.T., Wydner, K.L., Coleman, J.R., and Lawrence, J.B. (1999). Processing of endogenous pre-mRNAs in association with SC-35 domains is gene specific. J. Cell Biol. *144*, 617–629.

35. Zhao, J., Sun, B.K., Erwin, J.A., Song, J.J., and Lee, J.T. (2008). Polycomb proteins targeted by a short repeat RNA to the mouse X chromosome. Science *322*, 750–756. https://doi.org/10.1126/science.1163045.

36. Żylicz, J.J., Bousard, A., Žumer, K., Dossin, F., Mohammad, E., da Rocha, S.T., Schwalb, B., Syx, L., Dingli, F., Loew, D., et al. (2019). The implication of early chromatin changes in X chromosome inactivation. Cell *176*, 182–197.e23. https://doi.org/10.1016/j.cell.2018.11.041.

37. Almeida, M., Pintacuda, G., Masui, O., Koseki, Y., Gdula, M., Cerase, A., Brown, D., Mould, A., Innocent, C., Nakayama, M., et al. (2017). PCGF3/5-PRC1 initiates Polycomb recruitment in X chromosome inactivation. Science *356*, 1081–1084. https://doi.org/10.1126/science.aal2512.

38. Chu, C., Zhang, Q.C., da Rocha, S.T., Flynn, R.A., Bharadwaj, M., Calabrese, J.M., Magnuson, T., Heard, E., and Chang, H.Y. (2015). Systematic discovery of Xist RNA binding proteins. Cell *161*, 404–416. https://doi.org/10.1016/j.cell.2015.03.025.

39. Hall, L.L., Byron, M., Pageau, G., and Lawrence, J.B. (2009). AURKB-mediated effects on chromatin regulate binding versus release of XIST RNA to the inactive chromosome. J. Cell Biol. *186*, 491–507. https://doi.org/10.1083/jcb.200811143.

40. Rodermund, L., Coker, H., Oldenkamp, R., Wei, G., Bowness, J., Rajkumar, B., Nesterova, T., Susano Pinto, D.M., Schermelleh, L., and Brockdorff, N. (2021). Time-resolved structured illumination microscopy reveals key principles of Xist RNA spreading. Science *372*, eabe7500. https://doi.org/10.1126/science.abe7500.

41. Wutz, A., and Jaenisch, R. (2000). A shift from reversible to irreversible X inactivation is triggered during ES cell differentiation. Mol. Cell. *5*, 695–705.

42. Clemson, C.M., McNeil, J.A., Willard, H.F., and Lawrence, J.B. (1996). XIST RNA paints the inactive X chromosome at interphase: evidence for a novel RNA involved in nuclear/chromosome structure. J. Cell Biol. *132*, 259–275. https://doi.org/10.1083/jcb.132.3.259.

43. Hall, L.L., Byron, M., Sakai, K., Carrel, L., Willard, H.F., and Lawrence, J.B. (2002). An ectopic human XIST gene can induce chromosome inactivation in postdifferentiation human HT-1080 cells. Proc. Natl. Acad. Sci. USA *99*, 8677–8682. https://doi.org/10.1073/pnas.132468999.

44. Clemson, C.M., Hall, L.L., Byron, M., McNeil, J., and Lawrence, J.B. (2006). The X chromosome is organized into a gene-rich outer rim and an internal core containing silenced nongenic sequences. Proc. Natl. Acad. Sci. USA *103*, 7688–7693. https://doi.org/10.1073/pnas.0601069103.

45. Hall, L.L., Carone, D.M., Gomez, A.V., Kolpa, H.J., Byron, M., Mehta, N., Fackelmayer, F.O., and Lawrence, J.B. (2014). Stable C0T-1 repeat RNA is abundant and is associated with euchromatic interphase chromosomes. Cell *156*, 907–919. https://doi.org/10.1016/j.cell.2014.01.042.

46. Helbig, R., and Fackelmayer, F.O. (2003). Scaffold attachment factor A (SAF-A) is concentrated in inactive X chromosome territories through its RGG domain. Chromosoma *112*, 173–182. https://doi.org/10.1007/s00412-003-0258-0.

47. Ridings-Figueroa, R., Stewart, E.R., Nesterova, T.B., Coker, H., Pintacuda, G., Godwin, J., Wilson, R., Haslam, A., Lilley, F., Ruigrok, R., et al. (2017). The nuclear matrix protein CIZ1 facilitates localization of Xist RNA to the inactive X-chromosome territory. Genes Dev. *31*, 876–888. https://doi.org/10.1101/gad.295907.117.

48. Sunwoo, H., Colognori, D., Froberg, J.E., Jeon, Y., and Lee, J.T. (2017). Repeat E anchors Xist RNA to the inactive X chromosomal compartment

through CDKN1A-interacting protein (CIZ1). Proc. Natl. Acad. Sci. USA *114*, 10654–10659. https://doi.org/10.1073/pnas.1711206114.

49. Warder, D.E., and Keherly, M.J. (2003). Ciz1, Cip1 interacting zinc finger protein 1 binds the consensus DNA sequence ARYSR(0-2)YYAC. J. Biomed. Sci. *10*, 406–417. https://doi.org/10.1007/bf02256432.
50. Coverley, D., Marr, J., and Ainscough, J. (2005). Ciz1 promotes mammalian DNA replication. J. Cell Sci. *118*, 101–112. https://doi.org/10.1242/jcs.01599.
51. Swarts, D.R.A., Stewart, E.R., Higgins, G.S., and Coverley, D. (2018). CIZ1-F, an alternatively spliced variant of the DNA replication protein CIZ1 with distinct expression and localisation, is overrepresented in early stage common solid tumours. Cell Cycle *17*, 2268–2283. https://doi.org/10.1080/15384101.2018.1526600.
52. Kolpa, H.J., Creamer, K.M., Hall, L.L., and Lawrence, J.B. (2022). SAF-A mutants disrupt chromatin structure through dominant negative effects on RNAs associated with chromatin. Mamm. Genome *33*, 366–381. https://doi.org/10.1007/s00335-021-09935-8.
53. Colognori, D., Sunwoo, H., Wang, D., Wang, C.Y., and Lee, J.T. (2020). Xist repeats A and B account for two distinct phases of X inactivation establishment. Dev. Cell *54*, 21–32.e5. https://doi.org/10.1016/j.devcel.2020.05.021.
54. Engreitz, J.M., Pandya-Jones, A., McDonel, P., Shishkin, A., Sirokman, K., Surka, C., Kadri, S., Xing, J., Goren, A., Lander, E.S., et al. (2013). The Xist lncRNA exploits three-dimensional genome architecture to spread across the X chromosome. Science *341*, 1237973. https://doi.org/10.1126/science.1237973.
55. McHugh, C.A., Chen, C.K., Chow, A., Surka, C.F., Tran, C., McDonel, P., Pandya-Jones, A., Blanco, M., Burghard, C., Moradian, A., et al. (2015). The Xist lncRNA interacts directly with SHARP to silence transcription through HDAC3. Nature *521*, 232–236. https://doi.org/10.1038/nature14443.
56. Chen, C.K., Blanco, M., Jackson, C., Aznauryan, E., Ollikainen, N., Surka, C., Chow, A., Cerase, A., McDonel, P., and Guttman, M. (2016). Xist recruits the X chromosome to the nuclear lamina to enable chromosome-wide silencing. Science *354*, 468–472. https://doi.org/10.1126/science.aae0047.
57. Pasini, D., Malatesta, M., Jung, H.R., Walfridsson, J., Willer, A., Olsson, L., Skotte, J., Wutz, A., Porse, B., Jensen, O.N., and Helin, K. (2010). Characterization of an antagonistic switch between histone H3 lysine 27 methylation and acetylation in the transcriptional regulation of Polycomb group target genes. Nucleic Acids Res. *38*, 4958–4969. https://doi.org/10.1093/nar/gkq244.
58. Seto, E., and Yoshida, M. (2014). Erasers of histone acetylation: the histone deacetylase enzymes. Cold Spring Harbor Perspect. Biol. *6*, a018713. https://doi.org/10.1101/cshperspect.a018713.
59. Brockdorff, N. (2017). Polycomb complexes in X chromosome inactivation. Philos. Trans. R. Soc. Lond. B Biol. Sci. *372*, 20170021. https://doi.org/10.1098/rstb.2017.0021.
60. Petropoulos, S., Edsgärd, D., Reinius, B., Deng, Q., Panula, S.P., Codeluppi, S., Plaza Reyes, A., Linnarsson, S., Sandberg, R., and Lanner, F. (2016). Single-cell RNA-seq reveals lineage and X chromosome dynamics in human preimplantation embryos. Cell *165*, 1012–1026. https://doi.org/10.1016/j.cell.2016.03.023.
61. Jachowicz, J.W., Strehle, M., Banerjee, A.K., Blanco, M.R., Thai, J., and Guttman, M. (2022). Xist spatially amplifies SHARP/SPEN recruitment to balance chromosome-wide silencing and specificity to the X chromosome. Nat. Struct. Mol. Biol. *29*, 239–249. https://doi.org/10.1038/s41594-022-00739-1.
62. Jacobson, E.C., Pandya-Jones, A., and Plath, K. (2022). A lifelong duty: how Xist maintains the inactive X chromosome. Curr. Opin. Genet. Dev. *75*, 101927. https://doi.org/10.1016/j.gde.2022.101927.
63. Shin, J., Bossenz, M., Chung, Y., Ma, H., Byron, M., Taniguchi-Ishigaki, N., Zhu, X., Jiao, B., Hall, L.L., Green, M.R., et al. (2010). Maternal Rnf12/RLIM is required for imprinted X-chromosome inactivation in mice. Nature *467*, 977–981. https://doi.org/10.1038/nature09457.
64. Eltoukhy, A.A., Siegwart, D.J., Alabi, C.A., Rajan, J.S., Langer, R., and Anderson, D.G. (2012). Effect of molecular weight of amine end-modified poly(beta-amino ester)s on gene delivery efficiency and toxicity. Biomaterials *33*, 3594–3603. https://doi.org/10.1016/j.biomaterials.2012.01.046.
65. Zugates, G.T., Peng, W., Zumbuehl, A., Jhunjhunwala, S., Huang, Y.H., Langer, R., Sawicki, J.A., and Anderson, D.G. (2007). Rapid optimization of gene delivery by parallel end-modification of poly(beta-amino ester)s. Mol. Ther. *15*, 1306–1312. https://doi.org/10.1038/mt.sj.6300132.
66. Park, I.H., Arora, N., Huo, H., Maherali, N., Ahfeldt, T., Shimamura, A., Lensch, M.W., Cowan, C., Hochedlinger, K., and Daley, G.Q. (2008). Disease-specific induced pluripotent stem cells. Cell *134*, 877–886. https://doi.org/10.1016/j.cell.2008.07.041.
67. DeKelver, R.C., Choi, V.M., Moehle, E.A., Paschon, D.E., Hockemeyer, D., Meijsing, S.H., Sancak, Y., Cui, X., Steine, E.J., Miller, J.C., et al. (2010). Functional genomics, proteomics, and regulatory DNA analysis in isogenic settings using zinc finger nuclease-driven transgenesis into a safe harbor locus in the human genome. Genome Res *20*, 1133–1142. https://doi.org/10.1101/gr.106773.110.
68. Schindelin, J., Arganda-Carreras, I., Frise, E., Kaynig, V., Longair, M., Pietzsch, T., Preibisch, S., Rueden, C., Saalfeld, S., Schmid, B., et al. (2012). Fiji: an open-source platform for biological-image analysis. Nat Methods *9*, 676–682. https://doi.org/10.1038/nmeth.2019.
69. Bao, X., Lian, X., and Palecek, S.P. (2016). Directed endothelial progenitor differentiation from human pluripotent stem cells via wnt activation under defined conditions. Methods Mol. Biol. *1481*, 183–196. https://doi.org/10.1007/978-1-4939-6393-5_17.
70. Byron, M., Hall, L.L., and Lawrence, J.B. (2013). A multifaceted FISH approach to study endogenous RNAs and DNAs in native nuclear and cell structures. Curr Protoc Hum Genet. Chapter *4*, Unit 4 15. https://doi.org/10.1002/0471142905.hg0415s76.
71. McCarthy, D.J., Chen, Y., and Smyth, G.K. (2012). Differential expression analysis of multifactor RNA-Seq experiments with respect to biological variation. Nucleic Acids Res. *40*, 4288–4297. https://doi.org/10.1093/nar/gks042.

STAR★METHODS

KEY RESOURCES TABLE

REAGENT or RESOURCE	SOURCE	IDENTIFIER
Antibodies		
Anti-H3K27me3	Millipore Sigma	Cat# 07–449; RRID:AB_310624
Anti-UbH2A	Cell Signaling	Cat# 8240; RRID:AB_10891618
Anti-FK2 Ubiquitinylated Proteins	Affiniti	Cat# PW 8810
Anti-H4K20me	Abcam	Cat# ab9051; RRID:AB_306967
Anti-macroH2A	Millipore Sigma	Cat# 07–219; RRID:AB_310439
Anti-hnRNP-U	Abcam	Cat# ab20666; RRID:AB_732983
Anti-CIZ1	Santa Cruz	Cat# sc-393021
Anti-H3K27ac	Diagenode	Cat# C15200184; RRID:AB_2713908
Anti-SC-35	Millipore Sigma	Cat# S4045; RRID AB_477511
FitcAnti-Dig	Roche	Cat# 11207741910; RRID:AB_514498
Alexa Flour 594 Streptavidin	Thermo Fisher	Cat# S32356
Alexa Fluor 488 Streptavidin	Thermo Fisher	Cat# S32354; RRID:AB_2315383
Biological Samples		
HES1,2&3	Carol Ware, University of Washington, Stem Cell Core (Hall et al., 2008)[17]	N/A
E4.5 mouse Embryo	Ingolf Bach, UMass Chan Medical School Shin et al., 2010[63]	N/A
Irradiated Mouse Embryonic Fibroblasts (iMEFs)	R&D Systems	Cat# PSC001
Chemicals, Peptides, and Recombinant Proteins		
X chromosome Paint	ID Labs Biotechnology	Cat# IDR7023-5
Chromosome 21 Paint	Meta Systems, Newton MA	Cat# D-0321-100-FI
XIST Stellaris probe	Biosearch Technologies	Cat# VSMF-2429-5
Chromosome 7 Paint	Vysis	Cat# 1066-7B
hCot1	Millipore Sigma	Cat# 11581074001
Biotin-16-dUTP	Millipore Sigma	Cat# 11093070910
Digoxigenin-11-dUTP (Dig)	Millipore Sigma	Cat# 11093088910
Formaldehyde	Millipore Sigma	Cat# 47671
RNasin Plus RNase inhibitor	Promega	Cat# N2615
Triton X-100	Millipore Sigma	Cat# 11332481001
Paraformaldehyde	Ted Pella	Cat# 18505
PBAE (poly(β-amino ester)) C320	Daniel Anderson, MIT (Eltoukhy et al., 2012[64]; Zugates et al., 2007)[65]	N/A
Essential 8 medium	Thermo Fisher	Cat# A1517001
DMEM/F12	Thermo Fisher	Cat# 12660-012
Knockout Serum Replacement	Thermo Fisher	Cat# 10828-028
GlutaMAX	Thermo Fisher	Cat# 35050-061
Non-essential amino acids	Thermo Fisher	Cat# 11140-050
β-mercaptoethanol	Millipore Sigma	Cat# M3148
FGF-β	Millipore Sigma	Cat# GF446
Collagenase type IV	Thermo Fisher	Cat# 17104-019
Vitronectin (VTN-N) Recombinant	Thermo Fisher	Cat# A14700
UltraPure 0.5M EDTA, pH 8.0	Thermo Fisher	Cat# 15575020
MEM	Thermo Fisher	Cat# 11095-080

(*Continued on next page*)

Continued

REAGENT or RESOURCE	SOURCE	IDENTIFIER
FBS	Thermo Fisher	Cat# 16000044
5,6-Dichlorobenzimidazole 1-β-D-ribofuranoside (DRB)	Millipore Sigma	Cat# D1916
5-10uM trichostatin-A (TSA)	Millipore Sigma	Cat# T1952
Tautomycin	Millipore Sigma	Cat# 580551
Doxycycline	Clonetech Labs	Cat# 631311
Phosphate-buffered saline (PBS)	Fisher	Cat# BP3994
CHIR99021	Tocris	Cat# 4423
CD34 MicroBead Kit	Miltenyi Biotec	Cat# 130-100-453
EGM2	Lonza	Cat# CC-3162
Y-27632 Rho-associated protein kinases (ROCK) inhibitor	Tocris	Cat# 1254
XL-2-TOPO	Thermo Fisher	Cat# K8050
NEBuilder HiFi DNA Assembly Master Mix	New England Biolabs	Cat# E2621
Deposited Data		
Raw images to illustrate how dynamic range can impact detection of sparse zone	This study	http://omero.umassmed.edu:4080/webclient/?show=project-2466
RNA Seq experiments	(Moon and Lawrence, 2022)[21]	GEO:GSE166849
Experimental Models: Cell Lines		
Parental DS iPSC clone	G. Q. Daley, Children's Hospital Boston (Park et al., 2008)[66]	DS1-iPS4 RRID:CVCL_D012
Parental A clone (isogenic)	Jiang et al., 2013[19]	N/A
XIST transgenic clone 1 (isogenic)	Jiang et al., 2013[19]	N/A
XIST transgenic clone 5 (isogenic)	Jiang et al., 2013[19]	N/A
A-repeat transgenic (isogenic)	this study	pTRE3G-A-Repeat-EF1a-RFP::DYRK1A
H9 hESC	WiCell	Cat# WA09; RRID:CVCL_9773
mESC	Anton Wutz, Institute of Molecular Health Sciences ETH Zurich (Wutz et al., 2002)[25]	N/A
50Mb-1 myoblasts	Helen Blau, Stanford University (Smith et al., 1999)[34]	N/A
Tig1 (Female normal human lung primary fibroblast)	Coriell	Cat# AG06173; RRID:CVCL_0560
Oligonucleotides		
GGAAGATCTTCATGTCTG CGGCTCTAGAGCT	This study	Vector For
AAAGAAAAATTCTCTGCAGAAT TCCACCACACTGGA	This study	Vector Rev, MB34
AATTCTGCAGAGAATTTTTCTT TGGAATCATTTTTGGTGACA	This study	A-Repeat For
CCGATCGAAACATTTTTTCATC CATAAAAAGCACCGA	This study	A-Repeat Rev
GGATGAAAAAATGTTTCGATC GGCCGGATATCAC	This study	SV40 Poly A For, MB37
GCTGTCCCTCTAAGATACATTG ATGAGTTTGGACAAACCAC	This study	SV40 Poly A Rev
TGTATCTTAGAGGGACAGCCC CCCCCCAAA	This study	EF1 + RFP For

(*Continued on next page*)

Continued

REAGENT or RESOURCE	SOURCE	IDENTIFIER
AGGATCCTCAAGTACTTC CAGCGCCTGTG	This study	EF1 + RFP Rev
AGGCGCTGGAAGTACTTGAGG ATCCTGATCGAG	This study	BGH Poly A For
ACATGAAGATCTTCCCCAG CATGCCTGCTATT	This study	BGH Poly A Rev
GACCAGAACCCTGGACTTGC	This study	MB47
GAGGAGCAGGGTCAGAACAC	This study	MB52
Recombinant DNA		
pTRE3G-XIST	(Jiang et al., 2013)[19]	Addgene #149608
DYRK1A ZFN1&2	(Jiang et al., 2013)[19]	N/A
rtTA/puro	(Jiang et al., 2013)[19]	N/A
AAVS1 ZFN	DeKelver et al., 2010[67]	N/A
hXIST	Addgene	G1A, RRID: Addgene_24690
mXIST	Carolyn Brown, The University of British Columbia	plasmid XIST-MC2
DYRK1A	BACPAC Resources Center (BPRC)	BAC RP11-777J19
APP	BPRC	BAC RP11-910G8
USP25	BPRC	BAC RP11-840D8
CXADR	BPRC	BAC RP11-1150I14
COL18A1	BPRC	BAC RP11-867O18
A-repeat	Carolyn Brown, The University of British Columbia	p5′ XIST
RFP	System Biosciences	HR700PA-RFP
Topo-DSCR3	This study	MV1060, MV1062
Topo-HLCS	This study	MV1069-MV1071
Topo-TTC3	This study	MV1072-MV1076
Topo-PIGP	This study	MV1077
Software and Algorithms		
Image J-Fuji	Schindelin et al., 2012[68]	https://ImageJ.net/Fiji
Zen v2.3 Blue	Carl Zeiss AG	www.zeiss.com
GradPad Prism 9	GraphPad Software	www.graphpad.com

RESOURCE AVAILABILITY

Lead contact

Further information and requests for resources and reagents should be directed to and will be fulfilled by Lead Contact Jeanne Lawrence (Jeanne.Lawrence@umassmed.edu).

Materials availability

Reagents used in this study are available upon request from the lead contact.

Data and code availability

- Raw images to illustrate how dynamic range can impact detection of sparse zone can be found at Omero data: http://omero.umassmed.edu:4080/webclient/?show=project-2466. RNA Seq data can be found at GEO: GSE16684921
- This paper does not report original code.
- Any additional information required to reanalyze the data reported in this paper is available from the lead contact upon request.

EXPERIMENTAL MODEL AND SUBJECT DETAILS

Human cells

This study was mainly performed in iPSC derived from a 1-year old male with Down syndrome kindly provided by G.Q. Daley.[66] XIST-transgenic lines were accomplished and characterized in Jiang et al. (2013). A-repeat transgenic lines were accomplished for this study as described below. To illustrate certain points, other cell lines were used such as H9 hESC and female TIG-1 (normal human lung primary fibroblast). iPSCs and ESC were maintained on irradiated mouse embryonic fibroblasts (iMEFs) (R&D Systems, PSC001) in hiPSC medium containing DMEM/F12 supplemented with 20% Knockout Serum Replacement, 1mM glutamine, 100mM non-essential amino acids, 100mM β-mercaptoethanol and 10 ng/ml FGF-β at 37°C with 20% O_2 and 5% CO_2. Cultures were passaged every 5–7 days with 1 mg/ml of collagenase type IV. In later studies, cells were grown in Essential 8 medium on plates coated with vitronectin 0.5 μg/cm^2. Cells were passaged at 80% confluency every 3–4 days with 0.5mM EDTA. TIG-1 line was cultured in MEM 15% FBS. Cells were periodically tested for mycoplasma.

Expression of XIST and the A-repeat was induced with doxycycline (500 ng/ml) while maintained as pluripotent throughout the time course or switched to differentiation conditions at the start of dox treatment. Random differentiation was achieved by removing iPS cells from feeder layer and feeding with DMEM/F12, 4% Knockout Serum Replacement, 100mM Non-essential amino acids, 1mM L-glutamine, 100mM β-mercaptoethanol. iPS cells were differentiated into endothelial cells with Gsk3 inhibitor[21] in LaSR basal media (formulated from Bao 2016[69]) with 6μM CHIR99021 for the first two days. Endothelial precursor cells were purified using a CD34 MicroBead Kit (Miltenyi Biotec, cat# 130-100-453); and maintained in EGM2 (Lonza, cat# CC-3162) (with 5μM Y-27632 for the first day) on vitronectin coated plates. NPC differentiation was performed as.[20]

For inhibition of HDACs, trichostatin-A (TSA) was used under conditions tested to minimize toxiticy, at 10 μM for 4 h or 5 μM for 8 h. For transcriptional inhibition, cells were incubated with 50ug/ul 5,6-Dichlorobenzimidazole 1-β-D-ribofuranoside (DRB) for the times indicated. Tautomycin was used at 3uM for four hours to inhibit protein phosphatase 1, which was previously shown to disperse XIST RNA from chromatin. Cells treated with inhibitors were then fixed as indicated below for RNA FISH or IF.

Mouse cells

Male mouse J1 ES cells containing a doxycycline-inducible Xist cDNA transgene integrated on Chr-11 (clone #65)[25] were also briefly used to illustrate some points. These cells were maintained in DMEM (GIBCO), 15% fetal calf serum (FCS, Hyclone), on mitomycin inactivated (10ug/ml mitomycin C for 2 h at 37°C) STO fibroblast feeder cells (SNL76) that produce LIF from an ectopic transgene. mES cells were differentiated by removing colonies from feeders (through two, 30–45 min sequential separations of single cell suspension onto gelatinized flasks) and distributing them as a single cell monolayer on gelatinized (0.1% porcine skin gelatin) flasks in the presence of 100nM all-*trans*-retinoic acid. Xist RNA expression was induced with 1 μg/ml doxycycline at the same time. Time points were taken by trypsinizing the cells and plating them as a monolayer onto coverslips coated with CellTak (BD) (following manufacturers protocol) for 1 h before fixation.

METHOD DETAILS

pTRE3G-A-repeat-EF1a-RFP::DYRK1A plasmid

The A-Repeat, and backbone with arms to DYRK1A, were PCR amplified from pTRE3G-XIST.[19] The EF1αRFP was amplified from plasmid HR700PA-RFP (System Biosciences). The five PCR products were GIBSON assembled. Primer sequences are listed in table. **Inducible A-repeat cell line**: The inducible A-repeat transgene was targeted to the first intron of the DYRK1A locus in chromosome 21, the tet-transactivator was targeted to chromosome 19 AAV site in Down syndrome iPS cells as described in,[19] but using PBAE (poly(β-amino ester), C320 (generously provided by the Anderson Lab, MIT[64,65]). Briefly, the Down syndrome iPS cell parental line provided by G. Q. Daley (Children's Hospital Boston)[66] were grown to exponential phase and cultured in 10mM of Rho-associated protein kinases (ROCK) inhibitor (Calbiochem; Y27632) 24h before transfection. A total of 55 μg DNA including five plasmids (pTRE3G-A-Repeat-EF1a-RFP, DYRK1A ZFN1, DYRK1A ZFN2, rtTA/puro and AAVS1 ZFN) with 6:1 ratio of A-repeat:rtTA/puro were mixed with 1:20 ratio of PBAE Polymer and incubated with cells for 4 h. Cells were washed with media and kept overnight with Essential 8 medium and rock inhibitor. Cells were selected for puromycin resistance the next day. Clones expressing RFP (red fluorescence protein) were isolated. Expression of the A-repeat was induced with 500ug/ul doxycycline. Clones that lost RFP upon dox induction were used for this study. Expression of A-repeat was validated by RNA FISH and proper targeting by colocalization of the A-repeat and DYRK1A RNA foci by RNA FISH.

RFP and DYRK1 RNA were usually detected as separate but adjacent transcription foci. However, we noticed that upon dox induction, some A-repeat transcripts also contained downstream sequences for RFP and DYRK1A in a colocalizing focus, but this co-localized RFP/DYRK1A signal was restricted to the A-repeat transcription focus, and appeared only in the presence of dox, suggesting readthrough. Although this RFP/DYRK1A RNA read-though signal persisted in the presence of dox, the RFP protein was no longer present, indicating gene silencing. Thus, no functional mRNA for RFP or DYRK1A was expressed from this locus upon dox induction and gene silencing.

Cells kept in the presence of puromycin selection expressed the A-repeat transgene in almost 100% of cells. The frequency of cells expressing A-repeat dropped over time when grown in the absence of puromycin due to stochastic silencing of the tet-activator. These non-inducing cells were used as internal "non-expressing" controls for many experiments.

DNA and RNA FISH and immunostaining

These protocols were carried out as previously described.[42,70] Cells were fixed for RNA *in situ* hybridization as described in.[70] Briefly, cells cultured on coverslips were extracted with Triton X-100 for 3 min and fixed in 4% paraformaldehyde in phosphate-buffered saline (PBS) for 10 min. Cells were then dehydrated in 100% cold ethanol for 10 min and air-dried. Cells were then hybridized with biotin-11-dUTP or digoxigenin-16-dUTP (dig) labeled nick translated DNA probes. DSCR3, TTC3, PIG3, HLCS DNA probes were obtained by amplifying ~10Kb gene regions from the DS iPS genomic DNA and cloned into TOPO vector. A cold TOPO vector was added to the hybridization mixture of TOPO constructions to decrease background.

For hybridizations, 50ng of labeled probes with CoT-1 DNA competitor were resuspended in 100% formaldehyde, followed by denaturation at 80°C for 10 min. Hybridizations were performed in 1:1 mixture of denatured probes and 50% formamide hybridization buffer supplemented with 2U/μl of RNasin Plus RNase inhibitor for 3 h or overnight at 37°C. Cells were then washed three times for 20 min each, followed by detection with anti-dig or streptavidin fluorescently conjugated secondary antibody. DNA was stained with DAPI. In simultaneous DNA/RNA FISH (interphase targeting assay), cellular DNA was denatured and hybridization was performed with 1 U/μl of RNasin Plus RNase inhibitor to preserve RNA. For immunostaining with RNA FISH, cells were immunostained first with primary antibodies containing RNasin Plus and fixed in 4% paraformaldehyde after detection, before RNA FISH.

Most antibodies were diluted at 1:500 ratio. X chromosome was detected with whole chromosome paint probe (ID Labs Biotechnology), following manufacturer's instructions.

QUANTIFICATION AND STATISTICAL ANALYSIS

Experimental groups were compared using either "unpaired t test" or "two-way ANOVA" as indicated in figure legends. Error bars reflect the SD from the mean.

Transcriptomic data was generated for a different study.[21] Briefly, data was derived from 4 transgenic lines. NPC were produced as in[20] and collected for sequencing on differentiation-day 14 (dox at diff-day 0) while endothelial cells were differentiated with Gsk3 inhibitor as in[69] and collected for sequencing on diff-day 12. RNA seq analysis was performed using EdgeR,[71] using normalized cpm values. Figure uses log2 values.

Image analysis

Cells were imaged on a Zeiss AxioObserver 7, equipped with a 100× Plan-Apochromat oil objective (NA 1.4) and Chroma multi-band-pass dichroic and emission filter sets (Brattleboro, VT), with a Flash 4.0 LT CMOS camera (Hamamatsu). Z stacks were taken for each field to evaluate detectable transcription foci. To evaluate flXIST mediated repression of gene transcription by RNA FISH, the transcription focus of specific chr21 genes within the XIST RNA territory were compared to the other two homologous gene alleles for size and brightness of the RNA signal. When only two gene foci are detected, the undetected XIST-associated gene was considered "silenced". Since the A-repeat does not paint a chromosomal territory as does flXIST, silencing of a nearby gene was evaluated by comparing the frequency and intensity of the gene's transcription focus in the allele closest to the A-repeat RNA signal in the presence of doxycycline, to the frequency and intensity of the same gene allele closest to the RFP RNA signal in the absence of doxycycline. Images show a plane from the z stack or a MIP (indicated). CoT-1 RNA holes were quantified by RNA FISH and scored for absent or reduced CoT-1 RNA over the XIST RNA signal. Most experiments were carried out a minimum of 3 times, with typically 100–300 cells scored in each experiment. Key results were confirmed by at least two independent investigators. Enrichment of H3K27me2, H2AK119ub, CIZ1, H4K20me, & macroH2A were scored as "enriched", when the label over the XIST RNA territory was visibly higher than the nucleoplasmic background. Line scans were done in ImageJ (fiji v32 or 64) or ZEN 3.1 (profile function) and plotted in Prism 8–9. Microfluorimetry was performed in ImageJ (fiji v64). Thresholding was applied to images highlighting the signals to be measured. Area and intensity were calculated from those thresholded areas resulting in integrated density measurements. Heat maps were created with ImageJ (fiji v32). Heat maps for the A-repeat were not performed as there was no defined low-density zone outside the dense RNA focus. Images were minimally enhanced for brightness and contrast to resemble what was seen by eye through the microscope. Due to the low intensity of the sparse XIST RNA in the sparse-zone and the dynamic range between that and the transcription focus, the initial sparse spread of XIST RNA may often be missed if cells are only observed on a computer screen (with poor dynamic range) rather than by eye under a microscope. Sparse-zone XIST can also be missed in images that are processed too much, or by super-resolution techniques that often reduce sensitivity.